Spectroscopy and electronic structure of jet-cooled Al_2

Zhenwen Fu, George W. Lemire, Gregory A. Bishea, and Michael D. Morse
Department of Chemistry, University of Utah, Salt Lake City, Utah 84112

(Received 17 July 1990; accepted 10 September 1990)

Resonant two-photon ionization spectroscopy has been used to study the jet-cooled Al_2 molecule. The ground state has been conclusively demonstrated to be of $^3\Pi_u$ symmetry, deriving from the $\sigma_g^1\pi_u^1$ electronic configuration. High resolution studies have established the bond length of the $X\,^3\Pi_u$ state as $r_e(X\,^3\Pi_u) = 2.701 \pm 0.002$ Å. The third-law estimate of the Al_2 bond strength has been reevaluated using the observed and calculated properties of the low-lying electronic states to give $D_0^0(Al_2) = 1.34 \pm 0.06$ eV. In addition to the previously reported $E\ 2\,^3\Sigma_g^- \leftarrow X\,^3\Pi_u$ and $F\,3^3\Sigma_g^- \leftarrow X\,^3\Pi_u$ band systems, the $E'\,3^3\Pi_g \leftarrow X\,^3\Pi_u$, F''–X, F'–X, $G\,^3\Pi_g \leftarrow X\,^3\Pi_u$, $H'\,^3\Sigma_g^- \leftarrow X\,^3\Pi_u$, and $H\,^3\Delta_g \leftarrow X\,^3\Pi_u$ band systems have been observed for the first time. Bands of the G–X, H'–X, and H–X systems have been rotationally resolved and analyzed, providing rotational constants and electronic state symmetries for the upper states of these systems. A discussion of all of the experimentally known states of Al_2 is presented, along with comparisons to previous experimental and theoretical work.

I. INTRODUCTION

In the general field of metal cluster chemistry, a major aim is to understand the chemical bonding between metal atoms. For the one-electron *s*-block alkali and coinage metals, chemical bonding is easily understood (at least for dimers and trimers) as arising from the σ-type interactions between half-filled atomic *s* orbitals. Accordingly, one can always expect diatomic metals of this group to possess $^1\Sigma_g^+$ ground states, while triatomics are expected to possess $^2E'$ ground states in D_{3h} symmetry, and are expected to undergo a Jahn–Teller distortion. Such general trends are of great utility in guiding our thinking about the metal–metal chemical bond.

Among the *p*-block metals, chemical bonding is significantly more complicated because of the possibility of both $p\sigma$-type and $p\pi$-type chemical interactions. The competition between these two fundamentally distinct modes of bonding is particularly severe in the group IIIA metals, where the deficiency of electrons prevents the formation of both $p\sigma$ and $p\pi$ chemical bonds. In these metals the lone *p* electron may participate in σ bonds or π bonds, but not both. To fully understand the chemical bonding in such systems, we must learn under what conditions $p\sigma$ bonding is favored, and when $p\pi$ bonding may be significant. With these questions in mind we have undertaken a spectroscopic investigation of diatomic aluminum, Al_2.

In Al_2 the likely candidates for the ground state may be derived by placing the two $3p$ electrons in σ_g or π_u bonding orbitals, resulting in possible ground electronic configurations of (1) σ_g^2, giving a $^1\Sigma_g^+$ state, (2) $\sigma_g^1\pi_u^1$, giving $^1\Pi_u$ and $^3\Pi_u$ states, of which the $^3\Pi_u$ state is expected to lie lowest in energy, and (3) π_u^2, giving $^1\Sigma_g^+$, $^1\Delta_g$, and $^3\Sigma_g^-$ states, of which the $^3\Sigma_g^-$ state is expected to lie lowest in energy. Thus the three most likely candidates for the ground state of Al_2 are: σ_g^2, $^1\Sigma_g^+$; $\sigma_g^1\pi_u^1$, $^3\Pi_u$; and π_u^2, $^3\Sigma_g^-$. If $p\sigma$ bonding is strongly favored in Al_2, the ground state will be σ_g^2, $^1\Sigma_g^+$. If $p\sigma$ bonding is favored, but its strength is not sufficient to overcome the exchange stabilization of a triplet ($S = 1$) state, the ground state will be $\sigma_g^1\pi_u^1$, $^3\Pi_u$. If $p\pi$ bonding is favored over $p\sigma$ bonding, the Al_2 ground state will be π_u^2, $^3\Sigma_g^-$. Thus, in this molecule a determination of the ground electronic state will allow the relative importance of $p\sigma$ bonding and $p\pi$ bonding to be assessed. All three possible ground state assignments have been made in the literature, resulting in considerable confusion about the electronic structure of Al_2.

The earliest observed spectrum of Al_2 was reported by Zeeman in 1954, although the carrier of the spectrum was incorrectly identified as AlC.[1] The emission spectrum observed by Zeeman in a King furnace was subsequently reinvestigated by Ginter *et al.* in 1963,[2] and was shown to correspond to either a $^3\Sigma_u^- \rightarrow {}^3\Sigma_g^-$ or $^3\Sigma_g^+ \rightarrow {}^3\Sigma_u^+$ emission system of Al_2. The rotationally resolved emission system displayed the 7:5 intensity alternation characteristic of a homonuclear diatomic with nuclear spin $I = 5/2$, thereby establishing Al_2 as the carrier of the spectrum. On the basis of the method of excitation and the expected electron configurations of Al_2, the spectrum was assigned as $^3\Sigma_u^- \rightarrow {}^3\Sigma_g^-$, and it was assumed that the lower $^3\Sigma_g^-$ state was the ground state of Al_2.

Following this initial gas phase work, a period of 20 years elapsed before further spectroscopic investigations were reported on Al_2. In 1983 two matrix isolation investigations of Al_2 were reported,[3,4] but neither study found the absorption bands corresponding to the gas phase $^3\Sigma_u^-$–$^3\Sigma_g^-$ band system. Since these bands are intense in emission, but absent in absorption in low-temperature matrices, the assignment of π_u^2, $^3\Sigma_g^-$ as the ground state of Al_2 was cast into doubt. In one study a broad absorption centered about 14 300 cm^{-1} and a vibrationally resolved absorption system near 24 500 cm^{-1} were reported for Al_2 isolated in solid krypton, and a reassignment of the ground state as σ_g^2, $^1\Sigma_g^+$ was made.[3] The second matrix investigation also reported a vibrationally resolved absorption band near 24 500 cm^{-1} in Ar, Kr, and Xe matrices, along with higher energy band systems without resolved structure.[4] These higher energy band systems showed a pronounced matrix shift, and were

 0021-9606/90/248420-22$03.00

most conspicuous in krypton matrices, occurring at 35 000 and 45 000 cm^{-1} in Kr.[4]

In 1986 a magnetic deflection study was performed to ascertain the magnetic properties of the aluminum clusters.[5] It was conclusively shown that Al_2 is deflected in an inhomogeneous magnetic field, thereby excluding the σ_g^2, $^1\Sigma_g^+$ state as a candidate for the ground state. This observation, combined with a failure to observe the $^3\Sigma_u^- - ^3\Sigma_g^-$ emission band system in a resonant two-photon ionization (R2PI) study of jet-cooled aluminum clusters, led Fu *et al.*[6] to conclude that $\sigma_g^1\pi_u^1$, $^3\Pi_u$ is the ground state of Al_2. In an effort to provide more definitive evidence for the ground state of Al_2, we have extended our R2PI investigations into the ultraviolet region of the spectrum, where numerous band systems have now been located.

Concurrent with our investigations, Cai *et al.*[7] have applied the technique of laser-induced fluorescence to the aluminum dimer. Again, no evidence of the $^3\Sigma_u^- - ^3\Sigma_g^-$ band system was observed for jet-cooled diatomic aluminum. Two band systems, labeled *E–X* and *F–X*, were observed in the ultraviolet region, however, and these were both attributed to $^3\Sigma_g \leftarrow X\,^3\Pi_u$ transitions based on the multiplet splittings which were present. Although the rotational structure of these band systems was not completely resolved, a rotational contour analysis of the $E \leftarrow X$ band system suggested $r_e(X\,^3\Pi_u) \approx 2.70$ Å and $r_e(E\,^3\Sigma_g) \approx 2.99$ Å.

This confusing series of experimental studies has found its counterpart in theoretical investigations of the aluminum dimer. A number of Hartree–Fock self-consistent field investigations have found the $\sigma_g^1\pi_u^1$, $^3\Pi_u$ state to be the ground state.[8–10] This conclusion has been modified in some studies including configuration interaction, however, leading to a prediction of a π_u^2, $^3\Sigma_g^-$ ground state.[10,11] Theoretical investigations using a generalized valence bond–configuration interaction approach also find the π_u^2, $^3\Sigma_g^-$ state to be the ground state.[12] A local density functional formalism employing the $X\alpha$-LCAO method and an effective core potential finds $\sigma_g^1\pi_u^1$, $^3\Pi_u$ to be the ground state,[13] however, as do various multiconfiguration self-consistent-field methods including configuration interaction to varying degrees.[14–17] There are also a few theoretical investigations which simply assume the ground state of Al_2 to be π_u^2, $^3\Sigma_g^-$.[18,19] Despite the discrepancies between these various calculations, all of the theoretical studies of Al_2 are united in one respect: the σ_g^2, $^1\Sigma_g^+$ state is rejected as a candidate for the ground state. The only viable possibilities are π_u^2, $^3\Sigma_g^-$ and $\sigma_g^1\pi_u^1$, $^3\Pi_u$.

The most extensively correlated calculations on the aluminum dimer, employing the largest basis sets, have concluded that the ground state of Al_2 is $\sigma_g^1\pi_u^1$, $^3\Pi_u$.[16,17] The low-lying π_u^2, $^3\Sigma_g^-$ state is estimated to lie only about 170 cm^{-1} above the ground $\sigma_g^1\pi_u^1$, $^3\Pi_u$ state, however.[16,17] It is remarkable that theoretical methods and computational facilities have developed to the point that an energy difference of this magnitude, representing less than 0.0002% of the total energy of the Al_2 molecule,[17] is considered significant enough to provide an assignment of the ground electronic state.[16] In this paper we provide definite experimental confirmation that the theoretical assignment is correct, although we have no data to establish the magnitude of the $^3\Sigma_g^- - X\,^3\Pi_u$ energy separation.

The experimental methods used in this study are described in Sec. II, and our results are presented in Sec. III. A discussion of these results is given in Sec. IV, where comparisons to theoretical calculations and to the results of laser-induced fluorescence spectroscopy are made. Section V then concludes the paper with a summary of our findings.

II. EXPERIMENTAL

The molecular beam apparatus used in the present investigation of Al_2 is virtually identical to that used in previous studies of Al_3 (Ref. 6), Pt_2 (Ref. 20), C_3 (Ref. 21), NiCu (Ref. 22), GaAs,[23] and NiPt.[24] The metal cluster source utilizes a design similar to that developed by O'Brien *et al.*,[25] in which the second harmonic radiation (532 nm, 15–30 mJ/pulse) of a *Q*-switched Nd:YAG laser is focused onto a metal target disk located in the throat of a pulsed supersonic expansion of helium. In order to avoid drilling a hole in the metal target, it is continuously rotated and translated, so that a spiral pattern of metal is removed from its surface. In the present experiments machine shop aluminum was used as the target disk, since minor impurities were expected to be inconsequential given that a mass spectrometric detection scheme was used.

Downstream from the point of vaporization the helium and aluminum clusters expand into vacuum. The molecular beam is then skimmed, following which it enters the ionization region of a reflectron-type time-of-flight mass spectrometer. Spectra of the aluminum dimer are then recorded by monitoring the mass 54 ion signal as a frequency-doubled pulsed dye laser is scanned. All of the observed band systems of Al_2 lie higher in energy than 27 200 cm^{-1}, so absorption of one UV photon to excite the molecule, followed by absorption of a second UV photon of the same frequency energizes the Al_2 molecule with at least 6.74 eV of energy. The adiabatic ionization potential of Al_2 has recently been measured as 5.989 ± 0.002 eV,[26] so this amount of energy can readily ionize the molecule, thereby providing the mass spectrometric signal which is monitored. Because all of the observed band systems of Al_2 lie at energies more than halfway to the ionization limit, no second ionization laser is required.

The advantage of a one-color resonant two-photon ionization scheme such as that described above is that there are no problems associated with the temporal and spatial overlap of the resonant and ionization lasers, since both photons come from the same laser pulse. This, coupled with the fact that no additional laser is required, makes the one-color method very attractive. The disadvantage, however, is that it is difficult or impossible to measure excited state lifetimes by the method of time-delayed resonant two-photon ionization, since both photons come from the same laser beam. We have attempted to use KrF (248 nm, 5.00 eV), N_2 (337 nm, 3.68 eV), and XeF (353 nm, 3.51 eV) radiation as a second color in a time-delayed R2PI scheme to measure excited state lifetimes, but this has not been successful. All of these wavelengths are resonant with spectroscopic transitions in Al_2, leading to a strong Al_2^+ signal even in the absence of dye laser light tuned to a resonance. As a result we are unable to

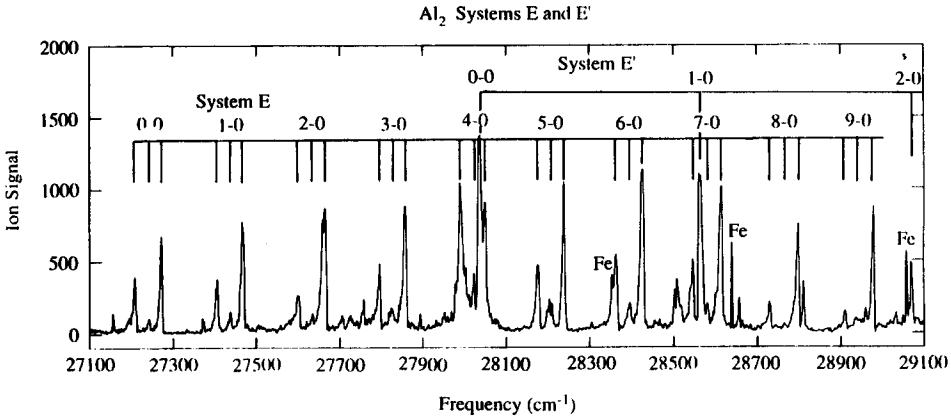

FIG. 1. The E–X and E'–X band systems of Al_2, recorded using frequency doubled LDS 698 and LDS 750 dye laser radiation. Based on a theoretical study of the excited states of Al_2 (Ref. 31), the upper states of these band systems are assigned as $E\,^3\Sigma_g^-$ and $E'\,^3\Pi_g$. They are the second and third states of their symmetry types, respectively. Sharp atomic transitions occurring in ^{54}Fe impurity atoms were used to calibrate the spectrum, and are labeled Fe in the spectrum

measure lifetimes for any of the excited states of Al_2 reported here.

The dye laser used in this work was pumped by the second or third harmonic of a Q-switched Nd:YAG laser, and its tunable output was frequency doubled using an angle-tuned potassium dihydrogen phosphate (KDP) or β-barium borate (BBO) doubling crystal. Low resolution scans were performed with a resolution of 1 cm^{-1} or better. High resolution scans (0.05 cm^{-1} FWHM in the second harmonic, ultraviolet output) were achieved by inserting an air-spaced etalon into the oscillator cavity, and pressure tuning the cavity with SF_6. Absolute frequency calibrations were accomplished in the high-resolution studies by simultaneously recording the spectrum of Al_2 and the absorption spectrum of gaseous I_2, for which the transition frequencies are precisely known.[27,28] Calibrations in low resolution scans were available from the atomic transitions of chromium and iron, which were present in small concentrations in the metal target. Frequencies of these transitions were calculated from the atomic energy levels as compiled by Charlotte Moore.[29]

III. RESULTS

A. Low resolution spectra of Al_2

Figures 1–7 display the band systems observed for jet-cooled Al_2, as recorded by the resonant two-photon ionization technique over the spectral range 27 100–40 200 cm^{-1}. Of the observed band systems, four show an obvious triplet of vibrational features which can only be explained as multiplet splittings in either the upper or lower state (Systems E, E'', F', and F). The remaining five band systems (Systems E', F'', G, H', and H) show only single vibrational features. Initially this led us to believe that both singlet and triplet states of Al_2 were populated in the molecular beam, and that the small spin–orbit interaction in this relatively light molecule prohibited efficient spin cooling in the expansion with helium. With the assumption that a metastable excited state of Al_2 might be more efficiently quenched by collisions with argon than with helium, spectra were obtained using argon carrier gas. Argon was found to collapse the obvious triplet systems (Systems E, E'', F', and F) to a single progression of subbands, but no substantial change in the intensity of the "triplet" band systems (E, E'', F', and F) as compared to the "singlet" band systems (E', F'', G, H', and H) was noted. Subsequent high-resolution studies of Systems G, H', and G (see Sec. III B below) clearly indicated that these band systems also correspond to triplet–triplet transitions. Contrary to our initial conclusions, we have no evidence of any metastable states of Al_2 populated in the supersonic expansion.

The high-resolution studies described below also demonstrated that System H' does *not* correspond to the $v'' = 1$ progression of hot bands associated with System H, but instead corresponds to excitation to a different upper elec-

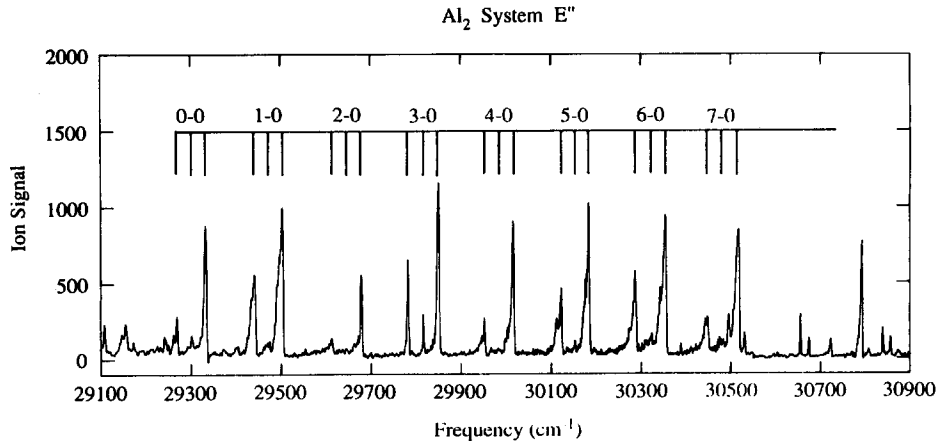

FIG. 2. The E''–X band system of Al_2, recorded using frequency doubled DCM and LDS 698 dye laser radiation. This band system is probably a continuation of the E–X system, as discussed in the text. However the E–X 10–0 band is anomalously weak, as is the E–X 13–0 band (E''–X 2–0 band in this figure). This may result from an avoided curve crossing which is evident in the calculated potential curves of Ref. 31, possibly leading to a fortuitous cancellation of transition moments for certain vibronic transitions. See the text for further discussion.

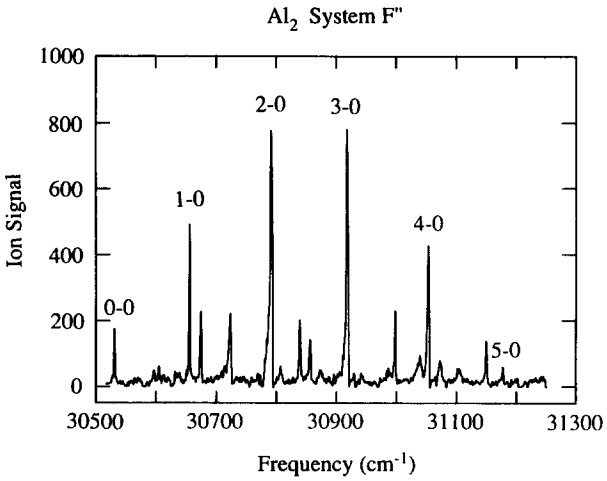

FIG. 3. The F''–X band system of Al_2, recorded using frequency doubled DCM dye laser radiation. This band system is somewhat irregular, with the 1–0 and 4–0 bands showing significant displacements from their expected positions (-4.60 and $+4.35$ cm^{-1}, respectively). The appearance of extra bands in this region suggests that the F'' $v=1$ and $v=4$ levels may be perturbed, thereby accounting for their displacements. Poor Franck–Condon factors may prevent observation of the 0–0 band, so the vibrational numbering is uncertain. The symmetry designation of the F'' state has not been established.

stead corresponds to excitation to a different upper electronic state. Thus our original interpretation that System H arises from a metastable singlet state of Al_2, with a vibrational frequency of $\Delta G''_{1/2} \approx 300$ cm^{-1} has been shown by high-resolution work to be in error. Although we had not published this interpretation, it has been quoted in Refs. 7 and 30. We retract this interpretation here. The evidence now indicates that all of the observed band systems originate from a common lower state, which is the ground state of Al_2. Spectroscopic constants obtained from the analysis of the low resolution data for the individual band systems are given in Table I.

The subband splittings found in the obvious triplet band systems E, E'', F', and F are constant within the error of the measurement from system to system and within the various vibrational levels of a given system. Using the data of Table I, the splitting between the highest and intermediate frequency subbands falls in the range 30.40 ± 0.42 cm^{-1}, while the splitting between the intermediate and lowest frequency subbands falls in the range 33.03 ± 0.51 cm^{-1}. The observed splitting between subbands includes contributions from the multiplet splittings of both the upper and lower states of the transition. Since all of the band systems originate from a common lower state, the constancy of the subband splittings therefore implies nearly identical multiplet splittings in the upper state of the E, E'', F', and F band systems. In general, there is no reason to expect the multiplet splitting in a set of excited electronic states to be constant within 1 cm^{-1} unless it is near zero in all of the states. On this basis we conclude that the upper states of the E, E'', F', and F band systems have very small multiplet splittings, and are probably best described in Hund's case (b). This conclusion is in agreement with the work of Cai *et al.*,[7] who assign the upper states of both the E and F band systems as $^3\Sigma_g$ (b) states. It is also in agreement with a recent detailed theoretical study of the spectroscopy of Al_2, where the upper states of the E and F band systems are assigned as the $2\,^3\Sigma_g^-$ and $3\,^3\Sigma_g^-$ states, respectively.[31]

With the multiplet splittings of the upper states of the E, E'', F', and F band systems assumed to be zero, the measured subband splittings must correspond to the multiplet splittings of the ground state of Al_2. Thus the Al_2 ground state is split into components with term energies of 0.0, 30.4, and 63.4 cm^{-1}. This pattern of term energies is *not* consistent with a π_u^2, $^3\Sigma_g^-$ ground state, which would be expected to show only a very slight splitting between its $\Omega'' = 0_g^+$ and $\Omega'' = 1_g$ components. It is precisely the pattern expected for a $\sigma_g^1\pi_u^1$, $^3\Pi_u$ ground state, however, which would split into $\Omega'' = 0_u^-$, 0_u^+, 1_u, and 2_u levels, with the $0_u^\pm$ pair of levels nearly equal in energy. This pattern of term energies in a $\sigma_g^1\pi_u^1$, $^3\Pi_u$ ground state would imply a spin–orbit interaction constant A for the ground state of Al_2 of approximately 31.7 cm^{-1}.[32] A semiempirical estimate of this parameter may be made using the method of Ishiguro and Kobori,[33] as described by Lefebvre-Brion and Field[34] to give

$$A = \zeta_{Al}(3p)/(2 + 2S_{AB}), \tag{3.1}$$

where S_{AB} is the overlap integral between $p\pi$ atomic orbitals centered on the two aluminum atoms and $\zeta_{Al}(3p)$ is the atomic spin–orbit constant, which is 74.7 cm^{-1} for atomic

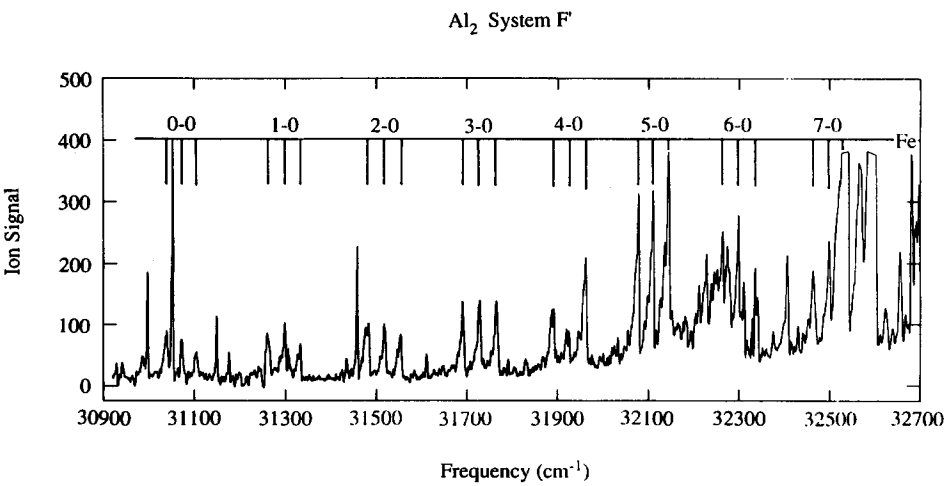

FIG. 4. The F'–X band system of Al_2, recorded using frequency doubled rhodamine 640 and DCM dye laser radiation. The triplets of bands observed here have the same spacing as in the E–X, E''–X, and F–X systems, indicating that the F' state of Al_2 has a tiny spin–orbit splitting, and must be considered in Hund's case (b). This system is extremely weak, with the 6–0 and 7–0 bands obscured by the 0–1 and 0–0 bands of the F–X system, respectively. Poor Franck–Condon factors may again prevent observation of the 0–0 band, so the vibrational numbering is uncertain. Other than belonging to Hund's case (b), no information concerning the symmetry of the F' state has been established. A transition in atomic ^{54}Fe at 32 680.03 cm^{-1} (labeled in the spectrum) was used to calibrate the frequency scale.

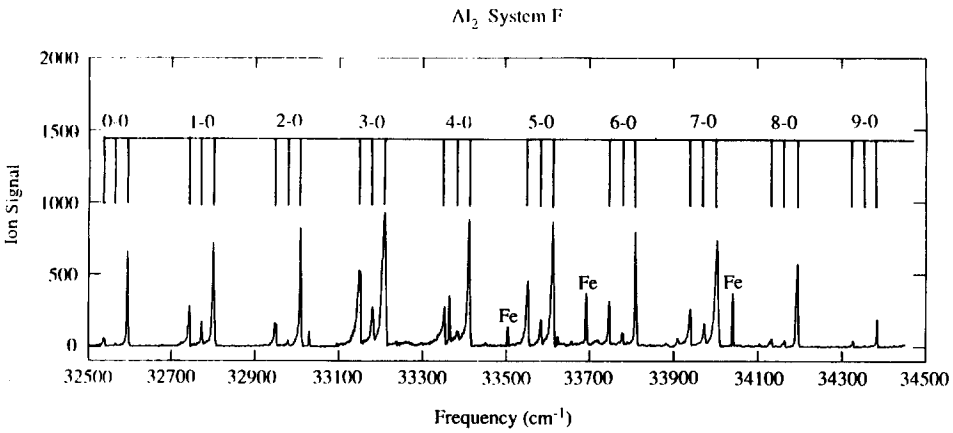

FIG. 5. The F–X band system of Al_2, recorded using frequency doubled rhodamine 590, 610, and 640 dye laser radiation. Based on a theoretical study of the excited states of Al_2 (Ref. 31), the upper state of this intense, regular band system may be assigned as $F\,^3\Sigma_g^-$, which is the third excited state of $^3\Sigma_g^-$ symmetry in Al_2. Transitions in atomic ^{54}Fe at 33 507.15, 33 695.42, and 34 039.54 cm^{-1} were used to calibrate the frequency scale in this spectrum.

aluminum.[34] The measured spin–oribt interaction constant, $A = 31.7\ cm^{-1}$, is consistent with the semiempirical estimate if the overlap integral S_{AB}, takes on the value $S_{AB} = 0.18$. This value is reasonable and tends to confirm the assignment of the ground state of Al_2 as $X\,^3\Pi_u$. A more definite confirmation is provided by the high-resolution studies described in Sec. III B below.

With this preliminary assignment of the ground state of Al_2, it is easy to understand why we observe so many band systems with triplets of subbands. It is more difficult to rationalize how the apparent singlet band systems arise. The upper states of these band systems cannot correspond to Hund's case (b), since we would then expect to see triplets of features corresponding to the spin–orbit splitting of the ground $^3\Pi_u$ state. With the exception of the H' band system, which is weak, and for which the other subbands may not be observed, we may be confident that the upper states of the E', F'', G, and H band systems belong to either Hund's case (a) or (c). Given the small spin–orbit constant $\zeta_{Al}(3p) = 74.7\ cm^{-1}$, and the fact that this parameter drops abruptly as n or l is increased, it is likely that the upper states of the apparent singlet bands belong to Hund's case (a). The upper states of these systems must then be of either $^3\Pi_g$ or $^3\Delta_g$ symmetry. Ungerade upper states and upper states with $\Lambda' > 2$ will not be optically accessible from a $^3\Pi_u$ ground state, and both

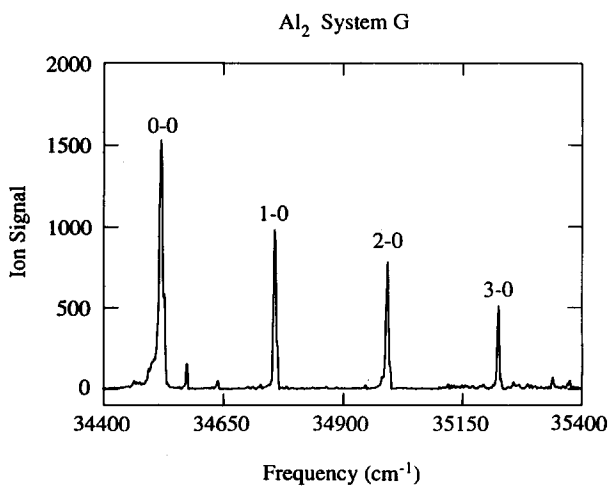

FIG. 6. The $G\,^3\Pi_g \leftarrow X\,^3\Pi_u$ band system of Al_2, recorded using frequency doubled fluorescein 548 and rhodamine 590 dye laser radiation. A high-resolution scan over the 2–0 band of this system is displayed in Fig. 8 below.

$^3\Sigma_g^-$ and $^3\Sigma_g^+$ should conform to Hund's case (b) and give a triplet of subbands. Despite these conclusions, the absence of observable subband structure is disturbing. This absence can be accounted for in either of two ways, however: (1) the upper state multiplet splitting may nearly match that of the ground state, so that the expected $\Delta\Omega = 0$ subbands of a $^3\Pi_g \leftarrow X\,^3\Pi_u$ transition and the $\Delta\Omega = +1$ subbands of a $^3\Delta_g \leftarrow X\,^3\Pi_u$ transition would fall on top of one another, leading to an apparent singlet band system, or (2) an Ω-selective predissociation may be occurring, so that only a single subband is detected in these resonant two-photon ionization experiments. Evidence from high-resolution studies suggests that overlapping subbands may account for the apparent singlet structure in the H band system, while the clean structure of System G in high resolution suggests that only the $\Omega' = 0_g^{\pm}$ components are immune to predissociation in this case.

The spectroscopic constants of Systems E and F, as obtained in the present study, are in good agreement with those reported by Cai *et al.*[7] Our measurements for System F, however, extend up to the 9–0 band, making our values of ω_e' and $\omega_e'x_e'$ slightly different from those reported previously.[7] Of greater interest, however, is the relationship between System E and System E''. We have had great difficulty in deciding whether these are two distinct band systems or one extended system. In System E we observe an obvious origin band and a progression of v'–0 bands up to $v' = 9$. The 10–0 band of System E is extremely weak, and the 0–0 band of System E'' appears close to where the 11–0 band of System E is expected. The remaining v'–0 bands of System E'' appear close to where the $(v' + 11)$–0 bands of System E are expected, and it is possible to combine the bands of Systems E and E'' into a single band system. With the exception of the 10–0 band, all of the v'–0 bands of the combined band system from $v' = 0$ to $v' = 18$ may be included in a fit. As shown in Table II, a fit of the highest frequency subbands ($^3\Sigma_g^- \leftarrow X\,^3\Pi_{0u}$) to an extended band system gives larger errors than are obtained when the systems are fit separately, but the errors are not unreasonable. The pattern of intensities in the extended band system is troubling, however, with the 10–0 and 13–0 bands anomalously weak. No stable isotopes other than ^{27}Al exist, which is unfortunate because the measurement of isotope shifts in the individual bands would resolve the question of one band system or two without any doubt. At this time we

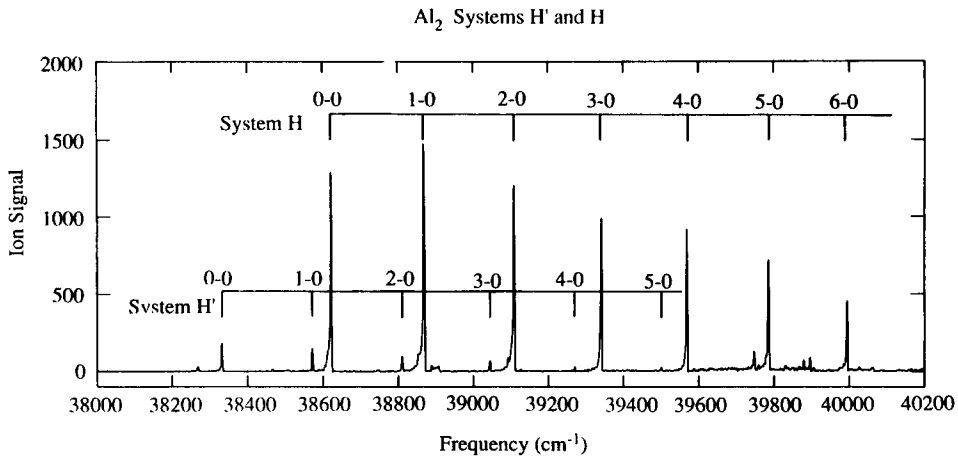

FIG. 7. The $H\,^3\Delta_g \leftarrow X\,^3\Pi_u$ and $H'\,^3\Sigma_g^- \leftarrow X\,^3\Pi_u$ band systems of Al_2, recorded using frequency doubled coumarin 500 dye laser radiation. High-resolution scans over the H–X 0–0 band and the H'–X 0–0 band are displayed in Figs. 9 and 10, respectively.

believe that System E'' is a continuation of System E, but further discussion of this point is deferred to Sec. IV, where a comparison to theoretical results[31] is made. In that section we also discuss the assignment of the upper electronic states of the observed transitions in detail.

B. High-resolution spectra of Al_2

After the low resolution spectra were recorded, attempts were made to rotationally resolve selected bands of the E, E', F, G, H' and H band systems. Systems E and E' fell into regions where the I_2 absorption spectrum[27,28] was unavailable for calibration, so relatively little time was spent on those attempts, and they met with no success. A large amount of time was spent on the F band system, since in this region the I_2 absorption spectrum provides an excellent calibration.[27,28] Unfortunately, the resolution of the frequency

TABLE I. Vibronic constants of Al_2 band systems.[a]

Band system	ν_{00}	ω_e'	$\omega_e'x_e'$	ΔE_{so}[b]	$\Delta G_{1/2,v}$	Number of observed bands[c]	Root mean square Error[d]
H–X	38 621.958 ± 0.002[e]	254.89 ± 0.31	3.64 ± 0.04			7 + 0	0.43
H'–X	38 328.248[e]	244.60 ± 1.78	1.80 ± 0.29			6 + 0	1.42
G–X	34 519.697 ± 0.004[e]	237.47 ± 1.91	0.41 ± 0.46			4 + 0	0.46
F_0–X	32 598.82 ± 0.66	209.83 ± 0.35	1.15 ± 0.03		285.97 ± 0.47	10 + 6	0.76
F_1–X	32 568.01 ± 0.32	210.28 ± 0.18	1.20 ± 0.02	30.81 ± 0.74		10 + 0	0.34
F_2–X	32 534.89 ± 0.64	209.92 ± 0.36	1.11 ± 0.04	33.12 ± 0.72		10 + 0	0.68
F_0'–X	31 101.62 ± 1.20	243.27 ± 1.08	5.85 ± 0.15			7 + 0	1.04
F_1'–X	31 070.83 ± 1.14	239.45 ± 1.03	5.36 ± 0.14	30.79 ± 1.65		7 + 0	1.70
F_2'–X	31 037.29 ± 0.92	236.29 ± 0.82	4.77 ± 0.12	33.54 ± 1.47		7 + 0	0.79
F''–X	30 530.36 ± 1.88[f]	129.93 ± 1.96[f]	0.10 ± 0.31[f]			6 + 0[f]	0.95[f]
E_0''–X	29 331.99 ± 1.41	175.78 ± 1.07	0.77 ± 0.13			8 + 0	0.13
E_1''–X	29 302.01 ± 1.40	175.38 ± 1.06	0.75 ± 0.13	29.98 ± 1.99		8 + 0	0.13
E_2''–X	29 269.49 ± 0.71	175.60 ± 0.54	0.83 ± 0.07	32.52 ± 1.57		8 + 0	0.67
E'–X	28 035.97[g]	551.85[g]	11.67[g]			3 + 0[g]	...
E_0–X	27 269.94 ± 0.86	199.54 ± 0.50	0.98 ± 0.05		290.76 ± 0.81	10 + 3[h]	0.95
E_1–X	27 239.78 ± 0.76	200.01 ± 0.46	1.08 ± 0.05	30.16 ± 1.15	286.52 ± 1.09	10 + 1[h]	0.71
E_2–X	27 206.96 ± 0.26	200.47 ± 0.16	1.14 ± 0.02	32.82 ± 0.81	282.87 ± 0.29	10 + 2[h]	0.25

[a] All constants are given in wave numbers (cm^{-1}).

[b] ΔE_{so} is defined as the energy difference between the ν_{00} values for the indicated members of a triplet band system.

[c] The first entry gives the number of bands observed originating from $v'' = 0$, while the second entry gives the number originating from $v'' = 1$.

[d] This is the root mean square deviation between the observed and fitted band positions.

[e] ν_{00} for the H–X, H'–X, and G–X band systems is taken from the high-resolution scans of the 0–0 bands of these systems, which were recorded while monitoring the absorption spectrum of I_2 at the fundamental of the frequency doubled dye laser. A correction was made to account for the Doppler shift experienced by the Al_2 molecules traveling at the beam velocity of helium (1.77×10^5 cm/s) toward the light source. This amounted to only $+0.228\ cm^{-1}$ for the H–X system, $0.226\ cm^{-1}$ for the H'–X system, and $+0.204\ cm^{-1}$ for the G–X system.

[f] Because of obvious perturbations (see the text), the 1–0 and 4–0 bands were omitted from the fit. They were also omitted from the calculation of the rms error.

[g] Because only three bands were observed, ν_{00}, ω_e', and $\omega_e'x_e'$ were uniquely determined, and no error estimate could be obtained.

[h] Because perturbations between the E' state and the $v' = 4$ and $v' = 7$ levels of the E state were suspected, the 4–0 and 7–0 bands were omitted from the fit of the E–X system.

TABLE II. Vibronic fits of the E and E'' band systems.[a]

	Fit as a single band system[b]			Fit as two band systems[c]		
Band head frequency	Assignment	Calculated frequency	Residual	Assignment	Calculated frequency	Residual
27 274.7	0–0 E–X	27 273.9	0.8	0–0 E–X	27 273.4	1.3
27 470.3	1–0 E–X	27 471.5	−1.2	1–0 E–X	27 471.0	−0.7
27 665.8	2–0 E–X	27 667.0	−1.2	2–0 E–X	27 666.7	−0.9
27 860.9	3–0 E–X	27 860.5	0.4	3–0 E–X	27 860.3	0.6
28 052.2	4–0 E–X	28 052.0	0.2	4–0 E–X	28 052.0	0.2
28 241.2	5–0 E–X	28 241.5	−0.3	5–0 E–X	28 241.8	−0.6
28 429.7	6–0 E–X	28 428.9	0.8	6–0 E–X	28 429.6	0.1
28 615.5	7–0 E–X	28 614.3	1.2	7–0 E–X	28 615.4	0.1
28 800.3	8–0 E–X	28 797.7	2.6	8–0 E–X	28 799.3	1.0
28 980.1	9–0 E–X	28 979.1	1.0	9–0 E–X	28 981.2	−1.1
29 335.8	11–0 E–X	29 335.8	0.0	0–0 E''–X	29 335.5	0.3
20 507.8	12–0 E–X	29 511.1	−3.3	1–0 E''–X	29 509.7	−1.9
29 684.2	13–0 E–X	29 684.3	−0.1	2–0 E''–X	29 682.5	1.7
29 855.0	14–0 E–X	29 855.6	−0.6	3–0 E''–X	29 853.6	1.4
30 022.4	15–0 E–X	30 024.8	−2.4	4–0 E''–X	30 023.3	−0.9
30 189.5	16–0 E–X	30 192.0	−2.5	5–0 E''–X	30 191.4	−1.9
30 359.0	17–0 E–X	30 357.2	1.8	6–0 E''–X	30 358.0	1.0
30 523.1	18–0 E–X	30 520.4	2.7	7–0 E''–X	30 523.0	0.1
27 375.3	2–1 E–X	27 376.2	−0.9	2–1 E–X	27 375.9	−0.6
27 759.9	4–1 E–X	27 761.2	−1.3	4–1 E–X	27 761.3	−1.4
27 953.0	5–1 E–X	27 950.7	−2.3	5–1 E–X	27 951.0	2.0

[a] All band frequencies are measured in wave numbers (cm^{-1}) at the band head. Transitions in atomic chromium and iron were used to calibrate the spectra, so the estimated uncertainty in the band positions is $\pm 3\ cm^{-1}$. The only subbands listed here originate from the $X\,^3\Pi_{0u}$ component, which is sufficient to compare the quality of the fits.

[b] Fitting the data as a single band system gives: $\nu_{00} = 27\,273.9 \pm 1.1\ cm^{-1}$, $\omega_e' = 199.58 \pm 0.30\ cm^{-1}$, $\omega_e'x_e' = 1.01 \pm 0.01\ cm^{-1}$, and $\Delta G''_{1/2} = 290.78 \pm 1.19\ cm^{-1}$, where the errors represent 1σ in the least-squares fit.

[c] Fitting the data as two band systems gives for the E–X system: $\nu_{00} = 27\,273.4 \pm 0.8\ cm^{-1}$, $\omega_e' = 199.54 \pm 0.50^{-1}$, $\omega_e'x_e' = 0.98 \pm 0.05\ cm^{-1}$, and $\Delta G''_{1/2} = 290.76 \pm 0.81\ cm^{-1}$. For the E''–X system: $\nu_{00} = 29\,335.5 \pm 1.4\ cm^{-1}$, $\omega_e' = 175.78 \pm 1.07\ cm^{-1}$, and $\omega_e'x_e' = 0.77 \pm 0.13\ cm^{-1}$. In both cases the errors represent 1σ in the least-squares fit.

doubled pulsed dye laser (certainly no better than 0.05 cm^{-1}) was not sufficient to resolve the individual rotational lines. Presumably this is a result of the complicated rotational structure of a $^3\Sigma_g^-$(b)$\leftarrow X\,^3\Pi_u$(a) band system, where the spin splitting of the $^3\Sigma_g^-$(b) upper state multiplies the number of rotational lines in the spectrum. Despite these failures on the lower-frequency band systems, high-resolution investigations of the G, H, and H' band systems were successful.

1. The $G^3\Pi_{0g} \leftarrow X\,^3\Pi_{0u}$ band system

High resolution studies of the G–X band system were performed on the 0–0 and 2–0 bands, revealing a very simple rotational structure, as shown in Fig. 8 for the 2–0 band. The spectra show only P and R branches, beginning with $P(1)$ and $R(0)$, thereby demonstrating that Ω is well-defined in both the upper and lower states and that $\Omega' = \Omega'' = 0$. A band head forms at about $R(13)$, indicating that the upper state bond length is increased from that of the ground state.

This high-resolution spectrum is consistent with a $^1\Sigma \leftarrow {}^1\Sigma$ transition except for one subtle point, and this contributed to our original erroneous interpretation of the apparent singlet band system as arising from a metastable $^1\Sigma$ state. The subtle point is that none of the high resolution scans performed on either the 0–0 or 2–0 bands of the G–X system displayed the 7:5 intensity alternation expected for a $^1\Sigma \leftarrow {}^1\Sigma$ transition in homonuclear diatomic with nuclear spin $I = 5/2$. The lack of an intensity alternation is consistent with an $\Omega' = 0 \leftarrow \Omega'' = 0$ transition, however, if both the

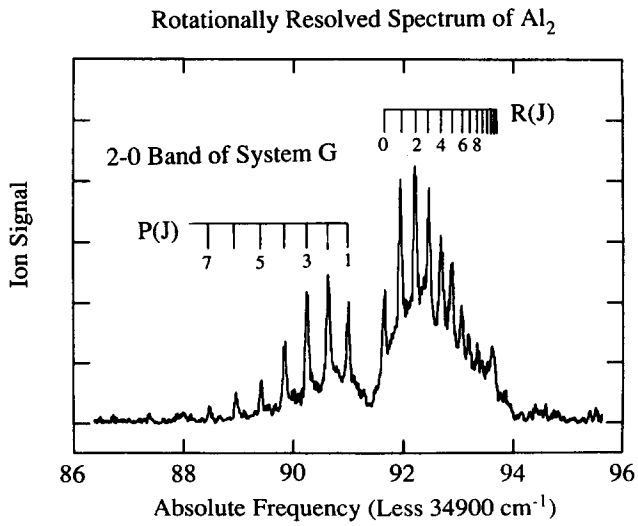

FIG. 8. The 2–0 band of the $G\,^3\Pi_{0g} \leftarrow X\,^3\Pi_{0u}$ band system, recorded in high resolution (0.05 cm^{-1}). The clear presence of P and R branches, and the absence of a Q branch confirm the band as an $\Omega' = 0 \leftarrow \Omega'' = 0$ transition, and the lack of an intensity alternation suggests that the $\Omega = 0^{\pm}$ lambda doubling is unresolved.

upper and lower states possess $\Omega = 0^+$ and $\Omega = 0^-$ components, and the Λ doubling which splits these two components is small or nearly equal in both states. In such a case the Λ doubling may be unobservable, and the intensity alternations in the $0^+ \leftarrow 0^+$ and $0^- \leftarrow 0^-$ transitions are opposite in sense, and cancel each other out. The presence of both 0^+ and 0^- components implies a triplet or higher multiplicity and requires Λ to be greater than or equal to 1. Given the likely candidates for the ground state of Al_2, as discussed in the Introduction, only $^3\Pi_u$ has both of the required 0^+ and 0^- components. Thus the high-resolution investigation of the *G–X* system provides further confirmation that $^3\Pi_u$ is the ground state of Al_2.

The observation of a strong $\Delta\Omega = 0$ subband originating from a $^3\Pi_u$ lower state implies in Hund's case (a) that the upper state is $^3\Pi_g$. On this basis the *G–X* band system is assigned as $G\,^3\Pi_{0g} \leftarrow X\,^3\Pi_{0u}$, although the expected $\Omega' = 1 \leftarrow \Omega'' = 1$ and $\Omega' = 2 \leftarrow \Omega'' = 2$ subbands have not been found. It is possible that an Ω-selective predissociation prevents their observation. Alternatively, the $\Omega' = 1 \leftarrow \Omega'' = 1$ and $\Omega' = 2 \leftarrow \Omega'' = 2$ subbands may overlap the $\Omega' = 0 \leftarrow \Omega'' = 0$ subband in low resolution, and the experimental conditions favoring low rotational temperatures which were employed in the high-resolution scans may have quenched the $^3\Pi_{1u}$ and $^3\Pi_{2u}$ components of the ground state.

The high-resolution spectra of the *G–X* 0–0 and 2–0 bands have been recorded while simultaneously monitoring the transmission of the dye laser fundamental light through a cell filled with gaseous I_2. Using the well-known I_2 absorption lines,[27,28] the resulting Al_2 spectra have been calibrated and line positions are accurately known to ± 0.02 cm^{-1}. Table III lists the measured and fitted line positions of the 0–0 and 2–0 bands of the *G–X* system. The line positions were fitted to the standard expression

$$\nu = \nu_0 + B'J'(J'+1) - B''J''(J''+1), \qquad (3.2)$$

from which effective values of B' and B'' were extracted for the $\Omega = 0$ levels of the $G\,^3\Pi_g$ and $X\,^3\Pi_u$ states. The results of these fits are provided in the footnotes in Table III.

2. The $H^3\Delta_{1g} \leftarrow X\,^3\Pi_{0u}$ band system

Deeper into the ultraviolet, the *H–X* band system also appears as an apparent singlet band system. High resolution studies of the 0–0 and 1–0 bands, however, definitely establish this as a triplet band system because the $\Omega'' = 0_u^+$ and

TABLE III. Observed and fitted line positions of the $G\,^3\Pi_{0g} \leftarrow X\,^3\Pi_{0u}$ system of Al_2.[a]

	0–0 band		2–0 band	
Assignment	Line position[a]	Residual[b,c]	Line position[a]	Residual[b,c]
R(10)	34 522.201	−0.009		
R(9)	34 522.070	−0.003		
R(8)	34 521.926	0.009	34 993.541	0.017
R(7)	34 521.758	0.014	34 993.377	−0.017
R(6)	34 521.554	0.003	34 993.242	0.000
R(5)	34 521.345	0.004	34 993.060	−0.006
R(4)	34 521.099	−0.014	34 992.868	0.001
R(3)	34 520.853	−0.013	34 992.644	0.000
R(2)	34 520.602	0.001	34 992.401	0.002
R(1)	34 520.314	−0.004	34 992.130	0.000
R(0)	34 520.026	0.009	34 991.839	0.001
P(1)	34 519.363	0.003	34 991.185	0.000
P(2)	34 518.999	−0.005	34 990.828	0.004
P(3)	34 518.635	0.005	34 990.439	0.000
P(4)	34 518.241	0.003	34 990.033	0.001
P(5)	34 517.848	0.020	34 989.603	0.002
P(6)	34 517.395	−0.004	34 989.146	−0.001
P(7)	34 516.972	0.019	34 988.666	−0.004
P(8)	34 516.456	−0.032		
P(9)	34 516.008	0.003		
P(10)	34 515.502	−0.001		
P(11)	34 514.978	−0.006		
P(12)	34 514.431	−0.015		
P(14)	34 513.315	−0.001		
P(15)	34 512.740	0.016		

[a] Line positions were measured by simultaneously recording the precisely known absorption spectrum of gaseous I_2, excited with the fundamental of the frequency doubled dye laser, and interpolating with the aid of a 0.2186 cm^{-1} free spectral range etalon. A correction of $+0.204$ cm^{-1} (0–0 band) or $+0.207$ cm^{-1} (2–0 band) was added to account for the Doppler shift of the Al_2 molecules as they move toward the light source.

[b] The $\Omega = 0^+, 0^-$ splitting was unresolved, so the observed lines were least-squares fitted to the formula $\nu = \nu_0 + B'J'(J'+1) - B''J''(J''+1)$, giving spectroscopic constants as follows (1σ error limits): 0–0 band: $\nu_0 = 34\,519.697 \pm 0.004$ cm^{-1}, $B_0'' = 0.168\,79 \pm 0.000\,17$ cm^{-1}, $B_0' = 0.159\,70 \pm 0.000\,19$ cm^{-1}; 2–0 band: $\nu_0 = 34\,991.523 \pm 0.003$ cm^{-1}, $B_0'' = 0.169\,08 \pm 0.000\,22$ cm^{-1}, $B_2' = 0.157\,50 \pm 0.000\,18$ cm^{-1}.

[c] Residuals are given as $\nu_{obs} - \nu_{calc}$.

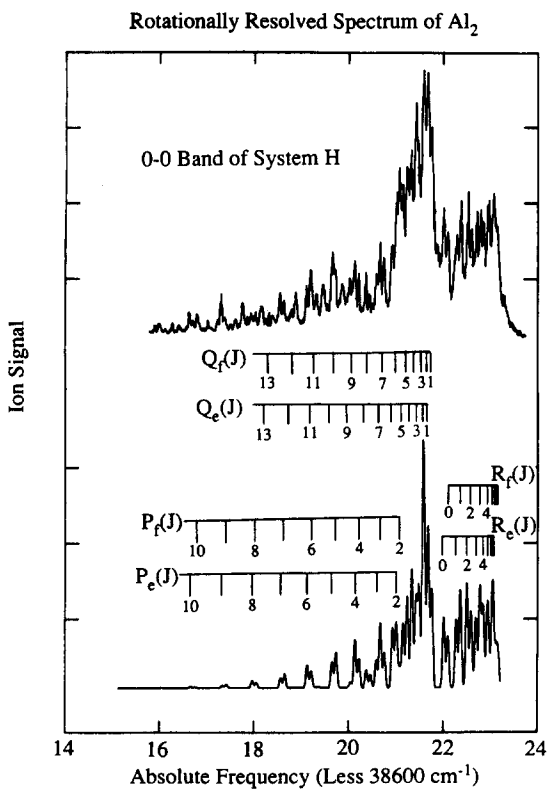

FIG. 9. The 0–0 band of the $H\,^3\Delta_{1g} \leftarrow X\,^3\Pi_{0u}$ band system, recorded in high resolution (0.05 cm^{-1}). In this band the lambda doubling of the $H\,^3\Delta_{1g}$ state is negligible, and the lambda doubling of the $X\,^3\Pi_{0u}$ state is just barely resolved. It is most evident in the $R(0)$, $R(1)$, and $R(2)$ lines, where the expected 7:5 intensity alternation is obvious. The lower panel displays a simulated spectrum, including the 7:5 intensity alternation.

0_u^- components of the ground state are resolved. This is clearly seen in Fig. 9 for the 0–0 band, where each R-branch line is doubled. Moreover, the 7:5 intensity alternation is now evident in the R branch, with $R_e(0)$ more intense than $R_f(0)$, $R_f(1)$ more intense than $R_e(1)$, etc. The observation of $R_e(0)$ and $R_f(0)$ establishes $\Omega' = 0$, while the obvious Q branch proves that $\Omega' = 1$. In Hund's case (a) an intense $\Omega' = 1 \leftarrow \Omega'' = 0$ subband is expected for either a $^3\Delta_g \leftarrow {}^3\Pi_u$ or a $^3\Sigma_g \leftarrow {}^3\Pi_u$ transition. In Al_2, however, we have little reason to expect that a $^3\Sigma_g$ state would fall into Hund's case (a). Accordingly, the H–X band system is assigned as $H\,^3\Delta_g \leftarrow X\,^3\Pi_u$, although the expected $\Omega' = 2_g \leftarrow \Omega'' = 1_u$ and $\Omega' = 3_g \leftarrow \Omega'' = 2_u$ subbands have not been clearly observed.

As shown in Fig. 9, the observed spectrum matches the simulated spectrum (lower panel) quite nicely in the R branch, but the observed spectrum displays additional structure in the P branch, and possibly in the Q branch as well. This structure very likely arises from the expected $\Omega' = 2_g \leftarrow \Omega'' = 1_u$ and $\Omega' = 3_g \leftarrow \Omega'' = 2_u$ subbands, which may be displaced slightly to the red of the $\Omega' = 1_g \leftarrow \Omega'' = 0_u^\pm$ subbands. These features are also weaker than the $\Omega' = 1_g \leftarrow \Omega'' = 0_u^\pm$ subband because the ground $^3\Pi_u$ state is regular, and the $\Omega'' = 1_u$ and $\Omega'' = 2_u$ levels are not populated as highly as the ground $\Omega'' = 0_u^\pm$ levels.

The small Λ doubling which separates the $^3\Pi_u$ $\Omega'' = 0_u^+$ and $\Omega'' = 0_u^-$ levels is observable in the R branch of the H–X 0–0 and 1–0 bands because the upper state $\Omega' = 1_g$ component has a Λ doubling which is small and only grows in with increasing J. Thus the splitting of the low-J R-branch lines which is evident in Fig. 9 provides a direct measurement of the splitting of the $\Omega'' = 0_u^\pm$ levels of the ground $X\,^3\Pi_u$ state. Moreover, the intensity alternation which is present in the R branch allows the sense of the Λ doubling to be determined. For the 0_u^+ component one expects states of even J to be more populated than states of odd J (7:5 ratio), while this is reversed for the 0_u^- component.[35] In Fig. 9 it is clear that the low-frequency member of the $R(0)$ and $R(2)$ doublets is more intense than the high frequency member. Accordingly, the low-frequency component of these doublets must originate from the 0_u^+ state, while the higher frequency component originates from the 0_u^- state. This places the $^3\Pi_u$ ($\Omega = 0_u^-$) substate lower in energy than the $^3\Pi_u$ ($\Omega = 0_u^+$) substate. From the measured splittings, the 0_u^- component of the $X\,^3\Pi_u$ ground state lies only about 0.08 cm^{-1} below the 0_u^+ component. In this connection it is interesting to note that a CASSCF calculation followed by relativistic configuration interaction calculations predicts a $^3\Pi_u$ ground state for the isovalent molecule In_2.[36] In this case the 0_u^- component is again stabilized relative to the 0_u^+ component, but to a much greater extent (231 cm^{-1})[36] than occurs in Al_2 (0.08 cm^{-1}).

Employing the usual expressions for the energies of the rotational levels in a $^3\Pi_0$ and a $^3\Delta_1$ state,[37,38]

$$
\begin{aligned}
{}^3\Pi_0\text{: } E(J,e/f) &= T_0^{(\Pi)} - A + 2\lambda/3 - 2\gamma \\
&\quad + B\,[J(J+1)+2] \mp (o+p+q), \\
{}^3\Delta_1\text{: } E(J,e/f) &= T_0^{(\Delta)} - 2A + 2\lambda/3 - 3\gamma \\
&\quad + B\,[J(J+1)+4] \mp \tilde{o}_\Delta J(J+1),
\end{aligned}
\tag{3.3}
$$

and collapsing the constant terms independent of J into substate origins gives

$$
\begin{aligned}
{}^3\Pi_0\text{: } E(J,e/f) &= T_0(^3\Pi_0) + BJ(J+1) \mp (o+p+q), \\
{}^3\Delta_1\text{: } E(J,e/f) &= T_0(^3\Delta_1) + BJ(J+1) \mp \tilde{o}_\Delta J(J+1).
\end{aligned}
\tag{3.4}
$$

These expressions have been used to extract the rotational and Λ-doubling constants for the $X\,^3\Pi_{0u}(v'' = 0)$ and $H\,^3\Delta_{1g}(v' = 0,1)$ substates by a least-squares fitting procedure. The measured and fitted line positions are given in Table IV, and the values of the fitted constants are provided in the footnotes of the table. The $\tilde{o}_\Delta$ constant, describing the Λ doubling in the $^3\Delta_{1g}$ state, was allowed to vary in the fit, but the resulting value was zero. A small value of $\tilde{o}_\Delta$ is expected, since Λ doubling in Δ states only arises in a fourth-order perturbation treatment of the portion of the Hamiltonian which is off-diagonal in Λ.[38]

3. The $H'\,^3\Sigma_g^- \leftarrow X\,^3\Pi_{0u}$ band system

A high-resolution study of the 0–0 band of the H'–X band system was also undertaken, with the intention of determining whether this system constituted a new band system, or comprised the $v'' = 1$ hot bands of the H–X system.

TABLE IV. Observed and fitted line positions for the $H\,^3\Delta_{1g} \leftarrow X\,^3\Pi_{0u}$ system of Al_2.[a]

	0–0 band[b]			1–0 band[c]		
Assignment	Line position[a]	Residual[d]	Comment	Line position[a]	Residual[d]	Comment
$R_e(0)$	38 622.221	0.005		38 869.019	−0.016	
$R_e(1)$	38 622.490	0.010		38 869.287	−0.007	
$R_e(2)$	38 622.713	0.006		38 869.510	−0.004	
$R_e(3)$	38 622.899	0.003		38 869.702	0.007	
$R_e(4)$	38 623.049	0.000		38 869.834	−0.003	
$R_e(5)$	38 623.156	−0.009		38 869.939	0.000	
$R_e(6)$			R_e head	38 870.004	0.002	
$R_f(0)$	38 622.300	−0.003		38 869.099	−0.018	
$R_f(1)$	38 622.573	0.006		38 869.370	−0.006	
$R_f(2)$	38 622.801	0.007		38 869.612	0.016	
$R_f(3)$	38 622.984	0.000		38 869.785	0.008	
$R_f(4)$			Blend with $R_e(5)$			Blend with $R_e(5)$
$R_f(5)$	38 623.250	−0.002				Blend with $R_e(6)$
$R_f(6)$	38 623.330	0.000				R_f head
$Q_{fe}(1)$	38 621.876	−0.001		38 868.683	−0.014	
$Q_{fe}(2)$	38 621.793	−0.010		38 868.619	0.001	
$Q_{fe}(3)$	38 621.676	−0.016		38 868.519	0.019	
$Q_{fe}(4)$	38 621.528	−0.015		38 868.343	0.000	
$Q_{fe}(5)$	38 621.361	0.004		38 868.145	−0.001	
$Q_{fe}(6)$	38 621.134	0.000		38 867.927	0.018	
$Q_{fe}(7)$	38 620.874	0.000				Blend with $P_f(3)$
$Q_{fe}(8)$	38 620.567	−0.010		38 867.291	−0.027	
$Q_{fe}(9)$	38 620.238	−0.005		38 866.977	0.012	
$Q_{fe}(10)$	38 619.872	0.001				
$Q_{fe}(11)$			Blend with $P_f(6)$			
$Q_{fe}(12)$	38 619.017	0.000				
$Q_{fe}(13)$	38 618.550	0.016				
$Q_{ef}(1)$	38 621.956	−0.009		38 868.759	−0.020	
$Q_{ef}(2)$	38 621.876	−0.015		38 868.687	−0.014	
$Q_{ef}(3)$			Blend with $Q_e(2)$			Blend with $Q_e(2)$
$Q_{ef}(4)$	38 621.634	0.003		38 868.451	0.026	
$Q_{ef}(5)$	38 621.460	0.015		38 868.219	−0.010	
$Q_{ef}(6)$	38 621.234	0.012				
$Q_{ef}(7)$	38 620.959	−0.003				
$Q_{ef}(8)$	38 620.674	0.009		38 867.389	−0.015	
$Q_{ef}(9)$	38 620.335	0.004		38 867.063	0.013	
$Q_{ef}(10)$			Blend with $Q_e(5)$			Blend with $Q_e(5)$
$Q_{ef}(11)$	38 619.546	−0.005				
$Q_{ef}(12)$	38 619.102	−0.003				
$Q_{ef}(13)$	38 618.616	−0.007				
$P_e(2)$			Blend with $Q_f(6)$	38 868.019	−0.002	
$P_e(3)$	38 620.799	0.011		38 867.611	0.007	
$P_e(4)$	38 620.335	−0.003		38 867.153	0.005	
$P_e(5)$			Blend with $Q_e(10)$	38 866.665	0.012	
$P_e(6)$	38 619.330	0.003		38 866.117	−0.001	
$P_e(7)$	38 618.766	0.000		38 865.540	−0.003	
$P_e(8)$	38 618.182	0.014		38 864.924	−0.007	
$P_e(9)$	38 617.531	−0.002				
$P_e(10)$	38 616.861	0.001				
$P_f(2)$	38 621.293	0.005		38 868.099	−0.004	
$P_f(3)$	38 620.874	−0.002	Blend with $Q_e(7)$	38 867.715	0.029	

TABLE IV. (*continued*).

	0–0 band[b]			1–0 band[c]		
Assignment	Line position[a]	Residual[d]	Comment	Line position[a]	Residual[d]	Comment
$P_f(4)$	38 620.429	0.003		38 867.233	0.003	
$P_f(5)$	38 619.934	−0.005	Blend with $Q_f(10)$	38 866.732	−0.002	
$P_f(6)$	38 619.415	0.000	Blend with $Q_e(11)$	38 866.210	0.010	
$P_f(7)$	38 618.859	0.005		38 865.625	−0.001	
$P_f(8)$	38 618.255	0.000		38 865.996	−0.015	
$P_f(9)$	38 617.614	−0.006				
$P_f(10)$	38 616.938	−0.009				

[a] All numerical values are given in wave numbers (cm^{-1}). Absolute line positions were obtained by simultaneously recording the precisely known absorption spectrum of gaseous I_2, excited with the fundamental of the frequency doubled dye laser, and interpolating with the aid of a 0.2186 cm^{-1} free spectral range etalon. A correction of $+0.228$ cm^{-1} (0–0 band) or $+0.229$ cm^{-1} (1–0 band) was added to account for the motion (1.77×10^5 cm/s) of the molecules toward the light source.

[b] The least-squares fit of the 0–0 band to Eqs. (3.4) gives $\nu_0 = 38\,621.9580 \pm 0.0015$ cm^{-1}, $B'_0 = 0.150\,59 \pm 0.000\,13$ cm^{-1}, $B''_0 = 0.169\,16 \pm 0.000\,13$ cm^{-1}, $(o+p+q)'' = -0.0438 \pm 0.0011$ cm^{-1}, and $\bar{o}'_\Delta = 0.0000 \pm 0.0000$ cm^{-1}. Errors represent 1σ in the fit.

[c] The least-squares fit of the 1–0 band to Eqs. (3.4) gives $\nu_0 = 38\,868.7780 \pm 0.0032$ cm^{-1}, $B'_1 = 0.149\,35 \pm 0.000\,32$ cm^{-1}, $B''_0 = 0.169\,02 \pm 0.000\,30$ cm^{-1}, $(o+p+q)'' = -0.0412 \pm 0.0022$ cm^{-1}, and $\bar{o}'_\Delta = 0.0000 \pm 0.0000$ cm^{-1}. Errors represent 1σ in the fit.

[d] Residuals are given as $\nu_{obs}-\nu_{calc}$.

The resulting high-resolution spectrum, shown in Fig. 10, is clearly the most complicated of the *G–X*, *H–X*, or *H'–X* systems. It shows little resemblance to the rotational structure of the *H–X* system shown in Fig. 9, and must constitute a new band system.

The spectrum is dominated by intense features near 38 328 cm^{-1}, which are presumably near the band origin. These have the appearance of *Q* branches, and are quite congested in structure. To the blue of these most intense features a regular series of closely spaced lines is found, becoming more closely spaced until a head is formed near 38 330 cm^{-1}. These features have the appearance of an *R* branch. Yet further to the blue another regular series of lines is found, with larger spacings than the previous series, again becoming more closely spaced as one moves to higher frequency. This has the appearance of an *S* branch. Finally, a regular series of lines is present to the red of the most intense features, although these are somewhat obscured by lines from other branches.

This complicated structure cannot be explained as either a $^3\Pi_g(a) \leftarrow X\,^3\Pi_u(a)$ or a $^3\Delta_g(a) \leftarrow X\,^3\Pi_u(a)$ transition. The only reasonable possibilities are that the upper state belongs to Hund's case (b), or that overlapping bands are present. With this in mind, we have attempted to analyze the band as a $^3\Sigma_g(b) \leftarrow X\,^3\Pi_u(a)$ transition. Although such a band should possess 27 branches, only 9 originate from the $X\,^3\Pi_{0u}$ state. Since the remaining 18 branches originate from the $\Omega'' = 1$ or 2 components of the ground state, significant supersonic cooling may have reduced their intensity substantially, preventing their observation. In any case a $^3\Sigma_g(b) \leftarrow X\,^3\Pi_{0u}(a)$ assignment of the subband shown in Fig. 10 would require the presence of P_{11}, P_{21}, P_{31}, Q_{11}, Q_{21}, Q_{31}, R_{11}, R_{21}, and R_{31} rotational branches.[32] The complicat-

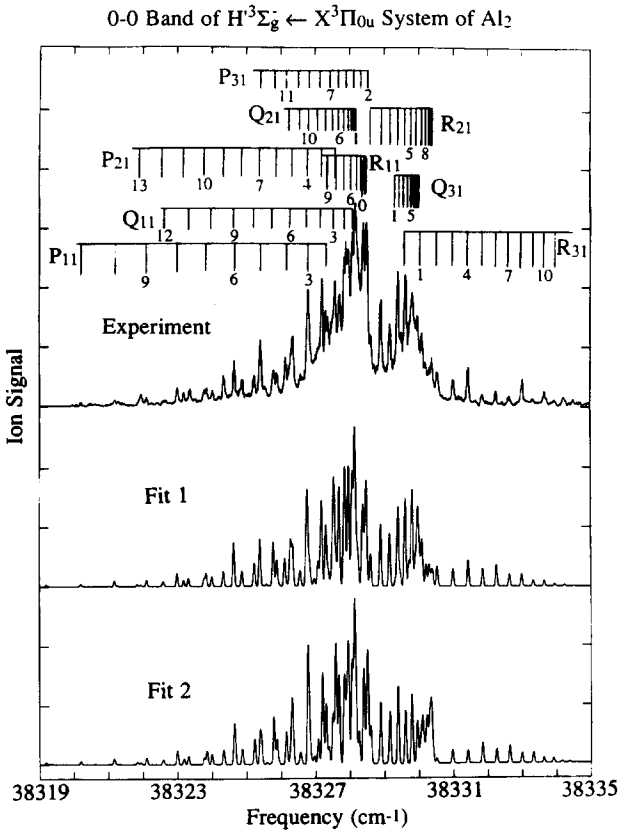

FIG. 10. The 0–0 band of the $H'\,^3\Sigma_g^- \leftarrow X\,^3\Pi_{0u}$ system, recorded in high resolution (0.05 cm^{-1}). Shown below this band are simulated spectra for Fit 1 and Fit 2. Both fits reproduce the low frequency portion of the spectrum very well, but Fit 1 gives the correct intensity alternation in the R_{31} branch, and reproduces the region near 38 330 cm^{-1} more faithfully. For these reasons Fit 1 is preferred. Individual line assignments based on the Fit 1 assignment are indicated over the experimental spectrum.

ed rotational structure of the H'–X 0–0 band shown in Fig. 10 can well be imagined to result from these nine rotational branches.

The rotational levels of the $X\,^3\Pi_{0u}$ state are primarily determined by the rotational quantum number J as indicated in Eq. (3.4). On the other hand, the rotational levels of a $^3\Sigma_g$(b) state are primarily determined by the nuclear rotational quantum number N which is weakly coupled with S to give J. This gives rotational levels specified by $F_1(N)$ for $J=N+1$, $F_2(N)$ for $J=N$, and $F_3(N)$ for $J=N-1$ as follows:[32]

$$\begin{aligned}
J=N+1\text{: } F_1(N) &= B_v N(N+1) + (2N+3)B_v - \lambda_v \\
&\quad - \sqrt{(2N+3)^2 B_v^2 - 2\lambda_v B_v + \lambda_v^2} \\
&\quad + \gamma_v(N+1), \\
J=N\text{: } F_2(N) &= B_v N(N+1), \\
J=N-1\text{: } F_3(N) &= B_v N(N+1) - (2N-1)B_v - \lambda_v \\
&\quad + \sqrt{(2N-1)^2 B_v^2 - 2\lambda_v B_v + \lambda_v^2} \\
&\quad - \gamma_v N. \qquad (3.5)
\end{aligned}$$

Here λ_v represents the direct spin–spin interaction between the two unpaired electrons, and also includes an important second-order spin–orbit contribution. Large values of λ_v lead to the breakdown of Hund's case (b) as the $^3\Sigma$ state splits into states with well-defined values of Ω, given by $\Omega = 1,0$. The spin–rotation interaction specified by γ_v is normally much smaller than λ_v.

With rotational energy levels primarily determined in the lower and upper states by J'' and N', respectively, transitions in which $N'=J''$ will have the appearance of Q branches. This is the case for the P_{31}, Q_{21}, and R_{11} branches. Likewise, the $N'=J''+1$ transitions (Q_{31} and R_{21} branches) will have the appearance of R branches. In similar fashion, the $N'=J''+2$ transitions (R_{31} branch) seem to form an S branch, the $N'=J''-1$ transitions (P_{21} and Q_{11} branches) seem to form P branches, and the $N'=J''-2$ transitions (P_{11} branch) seem to form an O branch. Thus the general structure of the H'–X 0–0 band displayed in Fig. 10 is consistent with a $^3\Sigma_g$(b) $\leftarrow X\,^3\Pi_{0u}$(a) band system.

With this possibility in mind, a subset of lines were sought within the H'–X 0–0 band corresponding to the P_{21} and R_{21} branches. These branches terminate on the F_2 component of the $^3\Sigma_g$ state, which has a particularly simple energy expression [see Eq. (3.5)]. Furthermore, they originate from only one of the $\Omega''=0$ components of the $X\,^3\Pi_{0u}$ state, leading again to a simple energy expression [see Eq. (3.4)]. Accordingly, the rotational structure encompassed by the P_{21} and R_{21} branches should have the appearance of simple P and R structure, with B'' equal to that determined for the G–X and H–X band systems. With these constraints the P_{21} and R_{21} branches were readily located, as listed in Table V.

Using the lines of the $P_{21}(J)$ and $R_{21}(J)$ branches given in Table V, and the values of B_0'' and $(o+p+q)_0''$ determined from the other high resolution investigations, the combination difference formulas[32,34]

$$Q_{21}(J) = R_{21}(J-1) - 2JB_0'' \mp 2(o+p+q)''$$

and

$$Q_{21}(J) = P_{21}(J+1) + (2J+2)B_0'' \mp 2(o+p+q)'' \qquad (3.6)$$

allowed the positions of the Q_{21} lines to be predicted. In these formulas the upper sign corresponds to a $^3\Sigma_g^+$ upper state, and the lower sign pertains to a $^3\Sigma_g^-$ upper state. The Q_{21} lines predicted by Eqs. (3.6) were then compared to the experimental spectrum, resulting in a definite assignment of the upper state as $H'\,^3\Sigma_g^-$.

With this assignment, the F_2 component of the $H'\,^3\Sigma_g^-$ state was completely accounted for. A number of lines below 38 326 cm^{-1} were not yet explained, however. In this region the P_{11} and Q_{11} branches should be present. Two regular series of lines were found in this region, and various assignments were attempted. Again, combination differences using the well-established ground state constants were used to verify or reject the possible assignments. Only one assignment was consistent in placing the R_{11} branch at the proper frequency. This branch forms the prominent head at 38 328.5 cm^{-1}, and provides a definite check on the validity of an assignment. The one assignment of the P_{11} and Q_{11} features which is acceptable in this regard is used in both Fit 1 and Fit 2, as given in Table V. This then accounted for the F_1 component of the $H'\,^3\Sigma_g^-$ state.

Finally, one must consider the F_3 component of the $H'\,^3\Sigma_g^-$ state, which leads to P_{31}, Q_{31}, and R_{31} branches. Of these branches, the R_{31} branch is most apparent in Fig. 10, where it forms the regular series of lines above 38 330.5 cm^{-1}. Simulated spectra show that the P_{31} and Q_{31} branches are quite weak, and fall in the ranges 38 326–38 329 cm^{-1} and 38 329–38 330 cm^{-1}, respectively. These weak branches tend to be obscured by more intense features in these ranges. This unfortunately leaves the R_{31} branch as the only source of information concerning the F_3 component of the $H'\,^3\Sigma_g^-$ state.

The R_{31} branch forms a regular series of lines above 38 330.5 cm^{-1}. Various possible numberings of this series of lines were attempted, and the results were again checked using combination differences to predict the locations of the P_{31} and Q_{31} branches. All but two possible numbering schemes placed the Q_{31} branch in a position where it would have been obvious in the spectrum. The two possible assignments differ in their numbering of the R_{31} branch by one, and both are listed in Table V. These form the basis for Fits 1 and 2, respectively. A higher resolution investigation, capable of resolving the P_{31} and Q_{31} lines from the more intense overlapping branches, would permit a definite assignment. This is beyond our present capabilities, however.

A straightforward application of formulas (3.5) for the energy levels of the $H'\,^3\Sigma_g^-$ state fails miserably to account for the observed spectrum, which cannot be fitted by the simple model implied by Eqs. (3.5). Given the large number of excited electronic states which are accessible at an energy of 38 000 cm^{-1} in Al_2, however, the failure of such a simple model should not be unexpected. Perturbations by other nearby states are not included in the model leading to Eqs.

TABLE V. Observed and fitted line positions for the 0–0 band of the $H'^3\Sigma_g^- \leftarrow X^3\Pi_{ou}$ system of Al_2.[a]

	Fit 1[b,c,e]			Fit 2[b,d,e]		
Line position	Assignment	Calculated frequency	Residual[f]	Assignment	Calculated frequency	Residual[f]
38 320.198	$P_{11}(11)$	38 320.212	−0.014	$P_{11}(11)$	38 320.199	−0.001
38 321.187	$P_{11}(10)$	38 321.184	0.003	$P_{11}(10)$	38 321.175	0.012
38 322.112	$P_{11}(9)$	38 322.113	−0.001	$P_{11}(9)$	38 322.110	0.002
38 322.997	$P_{11}(8)$	38 322.998	−0.001	$P_{11}(8)$	38 323.005	−0.008
38 323.841	$P_{11}(7)$	38 323.841	−0.000	$P_{11}(7)$	38 323.858	−0.017
38 324.645	$P_{11}(6)$	38 324.642	0.003	$P_{11}(6)$	38 324.669	−0.024
38 324.025	$Q_{11}(10)$	38 324.009	0.016	$Q_{11}(10)$	38 324.003	0.022
38 324.645	$Q_{11}(9)$	38 324.643	0.002	$Q_{11}(9)$	38 324.641	0.004
38 325.224	$Q_{11}(8)$	38 325.234	−0.010	$Q_{11}(8)$	38 325.238	−0.014
38 325.782	$Q_{11}(7)$	38 325.781	0.001	$Q_{11}(7)$	38 325.794	−0.012
38 323.184	$P_{21}(11)$	38 323.191	−0.007	$P_{21}(11)$	38 323.191	−0.007
38 323.787	$P_{21}(10)$	38 323.780	0.007	$P_{21}(10)$	38 323.779	0.008
38 324.347	$P_{21}(9)$	38 324.343	0.004	$P_{21}(9)$	38 324.342	0.005
38 324.885	$P_{21}(8)$	38 324.881	0.004	$P_{21}(8)$	38 324.879	0.006
38 325.414	$P_{21}(7)$	38 325.394	0.020	$P_{21}(7)$	38 325.392	0.022
38 325.880	$P_{21}(6)$	38 325.883	−0.003	$P_{21}(6)$	38 325.880	−0.000
38 326.327	$P_{21}(5)$	38 326.346	−0.019	$P_{21}(5)$	38 326.343	−0.016
38 326.787	$P_{21}(4)$	38 326.784	0.003	$P_{21}(4)$	38 326.781	0.006
38 327.193	$P_{21}(3)$	38 327.197	−0.004	$P_{21}(3)$	38 327.195	−0.002
38 327.573	$P_{21}(2)$	38 327.585	−0.012	$P_{21}(2)$	38 327.583	−0.010
38 327.690	$Q_{21}(6)$	38 327.684	0.006	$Q_{21}(6)$	38 327.681	0.009
38 327.826	$Q_{21}(5)$	38 327.834	−0.008	$Q_{21}(5)$	38 327.830	−0.004
38 327.957	$Q_{21}(4)$	38 327.959	−0.002	$Q_{21}(4)$	38 327.955	0.002
38 328.072	$Q_{21}(3)$	38 328.059	0.013	$Q_{21}(3)$	38 328.054	0.018
38 328.135	$Q_{21}(2)$	38 328.134	0.001	$Q_{21}(2)$	38 328.129	0.006
38 328.598	$R_{21}(0)$	38 328.600	−0.002	$R_{21}(0)$	38 328.598	−0.000
38 328.891	$R_{21}(1)$	38 328.888	0.003	$R_{21}(1)$	38 328.887	0.004
38 329.152	$R_{21}(2)$	38 329.151	0.001	$R_{21}(2)$	38 329.151	0.001
38 329.388	$R_{21}(3)$	38 329.389	−0.001	$R_{21}(3)$	38 329.390	−0.002
38 329.609	$R_{21}(4)$	38 329.603	0.006	$R_{21}(4)$	38 329.603	0.006
38 329.802	$R_{21}(5)$	38 329.791	0.011	$R_{21}(5)$	38 329.792	0.010
38 329.951	$R_{21}(6)$	38 329.954	−0.003	$R_{21}(6)$	38 329.957	−0.006
38 330.085	$R_{21}(7)$	38 330.092	−0.007	$R_{21}(7)$	38 330.096	−0.011
38 330.195	$R_{21}(8)$	38 330.205	−0.010	$R_{21}(8)$	38 330.210	−0.015
38 330.534	$R_{31}(2)$	38 330.527	0.007	$R_{31}(1)$	38 330.515	0.019
38 330.990	$R_{31}(3)$	38 330.986	0.004	$R_{31}(2)$	38 330.971	0.019
38 331.423	$R_{31}(4)$	38 331.427	−0.004	$R_{31}(3)$	38 331.418	0.005
38 331.843	$R_{31}(5)$	38 331.847	−0.004	$R_{31}(4)$	38 331.848	−0.005
38 332.239	$R_{31}(6)$	38 332.246	−0.007	$R_{31}(5)$	38 332.255	−0.016
38 332.614	$R_{31}(7)$	38 332.624	−0.010	$R_{31}(6)$	38 332.637	−0.023
38 332.990	$R_{31}(8)$	38 332.982	0.008	$R_{31}(7)$	38 332.994	−0.004
38 333.328	$R_{31}(9)$	38 333.320	0.008	$R_{31}(8)$	38 333.324	0.004
38 333.635	$R_{31}(10)$	38 333.639	−0.004	$R_{31}(9)$	38 333.627	0.008

[a] Line positions were measured by simultaneously recording the precisely known absorption spectra of gaseous I_2, excited with the fundamental of the frequency doubled dye laser, and interpolating with the aid of a 0.2164 cm^{-1} free spectral range etalon. A correction of $+0.226$ cm^{-1} was added to account for the Doppler shift experienced by the Al_2 molecules as they move toward the light source at a velocity of 1.77×10^5 cm/s.

[b] Fits 1 and 2 differ only in the numbering of the features of the R_{31} branch. This ambiguity results because neither the P_{31} nor the Q_{31} branch is resolved. See the text for details.

[c] Fitted constants for Fit 1: $\nu_0 = 38\,328.248$; $B_0'' = 0.169\,093$; $(o+p+q)_0'' = -0.038\,793$; $B_0'(0^+) = 0.142\,585$; $B_0'(1^+) = 0.156\,589$; $B_0'(1^-) = 0.163\,881$; $\lambda_0' = -0.327\,496$; $\gamma_0' = 0.049\,345$, giving $\chi^2 = 2.626\times10^{-3}$.

[d] Fitted constants for Fit 2: $\nu_0 = 38\,328.244$; $B_0'' = 0.169\,241$; $(o+p+q)_0'' = -0.040\,474$; $B_0'(0^+) = 0.159\,645$; $B_0'(1^+) = 0.156\,783$; $B'^0(1^-) = 0.145\,201$; $\lambda_0' = -0.568\,814$; $\gamma_0' = 0.026\,373$, giving $\chi^2 = 5.606\times10^{-3}$.

[e] The nonlinear least-squares algorithm employed here gives absurdly small error estimates, so no error estimates are reported for either fit.

[f] Residuals are given as $\nu_{obs}-\nu_{calc}$.

(3.5), and such effects are almost certainly present in Al_2 at 38 000 cm^{-1} of energy. With this in mind we have returned to Hougen's description[39] of the energy levels of a $^3\Sigma$ molecule to try to obtain a deeper understanding of the $H'^3\Sigma_g^-$ state of Al_2.

Using a parity-adapted Hund's case (a) basis set, Hougen[39] has derived the Hamiltonian matrix for the rotational levels of a $^3\Sigma$ molecule as

$$\mathbf{H} = \begin{pmatrix} BJ(J+1) & -2B\,[J(J+1)]^{1/2} & 0 \\ -2B\,[J(J+1)]^{1/2} & BJ(J+1)+2B-2\lambda & 0 \\ 0 & 0 & BJ(J+1) \end{pmatrix}, \tag{3.7}$$

TABLE VI. Line strength formulas for a $^3\Sigma(\text{int}) \leftarrow {}^3\Pi(\text{a})$ system.[a]

Branch[b]	General formula[c]	Case (b) limit $\lambda = \gamma = 0$[d]	Case (a) limit $\lambda \gg 0$[e]	$\Omega' \leftarrow \Omega''$	Case (a) limit $\lambda \ll 0$[e]	$\Omega' \leftarrow \Omega''$
$P_{11}(2)$	$\lvert c_1\rvert^2(J''-1)/4$	$J''(J''-1)/4(2J''-1)$	0	0←0	$(J''-1)/4$	1←0
$Q_{11}(1)$	$\lvert c_1\rvert^2(2J''+1)/4$	$(J''+1)/4$	0	0←0	$(2J''+1)/4$	1←0
$R_{11}(0)$	$\lvert c_1\rvert^2(J''+2)/4$	$(J''+2)^2/4(2J''+3)$	0	0←0	$(J''+2)/4$	1←0
$P_{21}(2)$	$(J''-1)/4$	$(J''-1)/4$	$(J''-1)/4$	1←0	$(J''-1)/4$	1←0
$Q_{21}(1)$	$(2J''+1)/4$	$(2J''+1)/4$	$(2J''+1)/4$	1←0	$(2J''+1)/4$	1←0
$R_{21}(0)$	$(J''+2)/4$	$(J''+2)/4$	$(J''+2)/4$	1←0	$(J''+2)/4$	1←0
$P_{31}(2)$	$\lvert c_2\rvert^2(J''-1)/4$	$(J''-1)^2/4(2J''-1)$	$(J''-1)/4$	1←0	0	0←0
$Q_{31}(1)$	$\lvert c_2\rvert^2(2J''+1)/4$	$J''/4$	$(2J''+1)/4$	1←0	0	0←0
$R_{31}(0)$	$\lvert c_2\rvert^2(J''+2)/4$	$(J''+1)(J''+2)/4(2J''+3)$	$(J''+2)/4$	1←0	0	0←0
$P_{12}(2)$	$\lvert c_2\rvert^2(J''+1)/2$	$(J''-1)(J''+1)/2(2J''-1)$	$(J''+1)/2$	0←1	0	1←1
$Q_{12}(1)$	$\lvert c_2\rvert^2(2J''+1)/2$	$J''/2$	$(2J''+1)/2$	0←1	0	1←1
$R_{12}(1)$	$\lvert c_2\rvert^2J''/2$	$J''(J''+1)/2(2J''+3)$	$J''/2$	0←1	0	1←1
$P_{22}(2)$	0	0	0	1←1	0	1←1
$Q_{22}(1)$	0	0	0	1←1	0	1←1
$R_{22}(1)$	0	0	0	1←1	0	1←1
$P_{32}(1)$	$\lvert c_1\rvert^2(J''+1)/2$	$J''(J''+1)/2(2J''-1)$	0	1←1	$(J''+1)/2$	0←1
$Q_{32}(1)$	$\lvert c_1\rvert^2(2J''+1)/2$	$(J''+1)/2$	0	1←1	$(2J''+1)/2$	0←1
$R_{32}(1)$	$\lvert c_1\rvert^2J''/2$	$J''(J''+2)/2(2J''+3)$	0	1←1	$J''/2$	0←1
$P_{13}(2)$	$\lvert c_1\rvert^2(J''+1)(J''+2)/4J''$	$(J''+1)(J''+2)/4(2J''-1)$	0	0←2	$(J''+1)(J''+2)/4J''$	1←2
$Q_{13}(2)$	$\lvert c_1\rvert^2(J''-1)(J''+2)(2J''+1)/4J''(J''+1)$	$(J''-1)(J''+2)/4J''$	0	0←2	$(J''-1)(J''+2)(2J''+1)/4J''(J''+1)$	1←2
$R_{13}(2)$	$\lvert c_1\rvert^2J''(J''-1)/4(J''+1)$	$J''(J''-1)(J''+2)/4(J''+1)(2J''+3)$	0	0←2	$J''(J''-1)/4(J''+1)$	1←2
$P_{23}(2)$	$(J''+1)(J''+2)/4J''$	$(J''+1)(J''+2)/4J''$	$(J''+1)(J''+2)/4J''$	1←2	$(J''+1)(J''+2)/4J''$	1←2
$Q_{23}(2)$	$(J''-1)(J''+2)(2J''+1)/4J''(J''+1)$	$(J''-1)(J''+2)(2J''+1)/4J''(J''+1)$	$(J''-1)(J''+2)(2J''+1)/4J''(J''+1)$	1←2	$(J''-1)(J''+2)(2J''+1)/4J''(J''+1)$	1←2
$R_{23}(2)$	$J''(J''-1)/4(J''+1)$	$J''(J''-1)/4(J''+1)$	$J''(J''-1)/4(J''+1)$	1←2	$J''(J''-1)/4(J''+1)$	1←2
$P_{33}(2)$	$\lvert c_2\rvert^2(J''+1)(J''+2)/4J''$	$(J''-1)(J''+1)(J''+2)/4J''(2J''-1)$	$(J''+1)(J''+2)/4J''$	1←2	0	0←2
$Q_{33}(2)$	$\lvert c_2\rvert^2(J''-1)(J''+2)(2J''+1)/4J''(J''+1)$	$(J''-1)(J''+2)/4(J''+1)$	$(J''-1)(J''+2)(2J''+1)/4J''(J''+1)$	1←2	0	0←2
$R_{33}(2)$	$\lvert c_2\rvert^2J''(J''-1)/4(J''+1)$	$J''(J''-1)/4(2J''+3)$	$J''(J''-1)/4(J''+1)$	1←2	0	0←2

[a] As in the case for the related Hönl–London factors, the strength of a rotational line in a spectrum is proportional to the line strength given above times a Boltzmann factor of $\exp[-E(J'',\Omega'')/kT]$. The degeneracy factor of $(2J''+1)$ has been absorbed into the line strength, as defined here.

[b] The first line of each branch is denoted by the value of J'' given in parentheses.

[c] The coefficients c_1 and c_2 are obtained from the diagonalization of the 2×2 portion of the Hamiltonian matrix (3.8), and provide the coefficients of the F_1 wave function as $\psi(F_1) = c_1\phi(\Omega = 1^+) + c_2\phi(\Omega = 0^+)$, where the ϕ's are the normalized, parity-adapted case (a) basis functions used to set up the Hamiltonian. The normalization requirement forces $|c_1|^2 + |c_2|^2 = 1$.

[d] In the case (b) limit all rotational constants in (3.8) are set equal, and λ and γ are set to zero.

[e] In the case (a) limit listed here, the Hamiltonian matrix of (3.7) is used, and λ is allowed to approach $\pm\infty$. In either limit Ω' becomes a good quantum number, and certain branches go to zero intensity. These correspond to cases in which the Hund's case (a) selection rule for a $^3\Sigma \leftarrow {}^3\Pi$ transition ($\Delta\Omega = \pm 1$) is violated, as listed above.

where certain terms have been incorporated into the electronic energy to simplify the form of the matrix. This matrix has been block-diagonalized according to parity, with the 1×1 block in the lower right corner corresponding to the f levels of a $^3\Sigma_g^-$ state, which provide the F_2 component of the $^3\Sigma_g^-$ ($\Omega=1_g$) state, with parity given as $-(-1)^J$.[34] The central element of the matrix gives the zeroth-order energy of the $^3\Sigma_g^-$ ($\Omega=0_g^+$) component of the $^3\Sigma_g^-$ state, which is shifted in energy relative to the $\Omega=1_g$ components by the term involving λ. This term usually results mainly from second-order spin–orbit effects, although spin–spin interactions make some contribution.[34] The element in the upper left corner of this matrix corresponds to the zeroth-order energy of the e levels of the $^3\Sigma_g^-$ ($\Omega=1_g$) state, which are coupled to the e levels of the $^3\Sigma_g^-$ ($\Omega=0_g^+$) state by the spin-uncoupling operator,[34,39] resulting in the off-diagonal matrix elements indicated above.

The Hamiltonian matrix (3.7) is not rigorously correct, however, as has been discussed in Hougen's monograph.[38] In particular, the values of B occurring in the various matrix elements of (3.7) are not precisely equal. For example, the value of B occurring in the (2,2) position corresponds to the expectation value of $\hbar^2/2\mu R^2$ evaluated for the $^3\Sigma_g^-$ ($\Omega=0_g^+$) component, while the values in the (1,1) and (3,3) positions correspond to the expectation value of this operator evaluated for the $^3\Sigma_g^-$ ($\Omega=1_g$) component. In principle, these values of b will differ, particularly for molecules with large spin–orbit interactions. In addition, off-diagonal S-uncoupling and L-uncoupling interactions with other electronic states may cause the various B values in Eq. (3.7) to take on different effective values, in much the same way that lambda doubling occurs. With these ideas in mind we have modified the effective Hamiltonian of Eq. (3.7) to give a new effective Hamiltonian

$$\mathbf{H}=\begin{pmatrix} B(1^+)J(J+1) & -2(B(1^+)-\gamma/2)[J(J+1)]^{1/2} & 0 \\ -2[B(1^+)-\gamma/2][J(J+1)]^{1/2} & B(0^+)J(J+1)+2B(0^+)-2\lambda & 0 \\ 0 & 0 & B(1^-)J(J+1) \end{pmatrix}, \tag{3.8}$$

where $B(1^+)$, $B(0^+)$, and $B(1^-)$ may take on different values. When $B(1^+)$, $B(0^+)$, and $B(1^-)$ take on the same value, this Hamiltonian reproduces the simple energy levels given by Eq. (3.5), as has been shown by Hougen.[39]

With the line assignments given in Table V, a nonlinear least-squares fit of the parameters ν_0, B_0'', $(o+p+q)_0''$, $B_0'(1^+)$, $B_0'(0^+)$, $B_0'(1^-)$, λ_o', and γ_0' has been successful in reproducing the spectrum. This is evident from the small residuals listed for Fit 1 and Fit 2 in Table V, and from the small values of χ^2 obtained. Figure 10 displays the experimental spectrum of the $H'\,^3\Sigma_g^- \leftarrow X\,^3\Pi_{ou}$ 0–0 band along with simulated spectra obtained using the parameters of Fit. 1 and Fit 2. Clearly both fits provide an excellent simulation of the experimental spectrum. For these simulations it was necessary to derive general line strength formulas for a $^3\Sigma$(intermediate) $\leftarrow$ $^3\Pi$(a) transition. These are given in Table VI along with the limiting forms which evolve as the $^3\Sigma$ state approaches case (b) or case (a).

The two simulated spectra shown in Fig. 10 reproduce the observed spectrum very well. The only major difference between these two simulations lies in the sense of the intensity alternation in the R_{31} branch. Although the experimental data are somewhat ambiguous on this point, it would appear that Fit 1 is more accurate in its reproduction of the experimental intensity pattern. In addition, Fit 1 shows a somewhat better agreement with the experimental data near the R_{21} band head at 38 330 cm^{-1}. The value of χ^2 resulting from Fit 1 is also somewhat better than that obtained from Fit 2. On this basis we conclude that Fit 1 is probably the correct assignment. Observation of the P_{31} and Q_{31} lines with a higher resolution laser would allow the assignment to be verified without ambiguity.

IV. DISCUSSION

A. Electronic states of Al_2

Previous experimental studies on Al_2, mainly by Ginter *et al.*[2] and Cai *et al.*,[7] along with the detailed theoretical investigation by Langhoff and Bauschlicher[31] and the present work, have provided characterizations of many of the electronic states of Al_2. In some cases there are discrepancies between the various experimental techniques, and between theory and experiment. In this section we summarize our current experimental knowledge of this molecule, and discuss the comparisons between the various experiments and theory for the known electronic states of Al_2. Spectroscopic constants for these states are summarized in Table VII, and experimentally based potential energy curves are given in Fig. 11.

1. The $X\,^3\Pi_u$ state

As discussed in Sec. III, the evidence is now overwhelming that the ground state of Al_2 arises from the $\sigma_g^1\pi_u^1$ electronic configuration, with electron spins triplet coupled to give the $^3\Pi_u$ term. The emergence of the $\sigma_g^1\pi_u^1$, $^3\Pi_u$ state as the ground electronic state of Al_2 is consistent with $p\sigma$ bonding being slightly favored over $p\pi$ bonding in this molecule.

The spin–orbit intervals between the $\Omega=0$, 1, and 2 states of Al_2 are slightly asymmetric, with the $\Omega=0$–$\Omega=1$ interval (30.4 cm^{-1}) slightly smaller than the $\Omega=1$–$\Omega=2$ interval (33.0 cm^{-1}). This asymmetry may be attributed to off-diagonal spin–orbit interactions between the $X\,^3\Pi_u$ state and higher electronic states. According to second-order perturbation theory, spin–orbit coupling to a higher-lying state (Y) will lower the energy of a given com-

TABLE VII. Electronic states of $^{27}Al_2$.[a]

State	T_0[b]	ω_e	$\omega_e x_e$	B_e	α_e	r_e(Å)
$H^3\Delta_{1g}$	38 621.958(2)[c]	254.9(3)	3.64 (4)	0.151 21(22)[c,d]	0.001 24(35)[c]	2.8747(21)[d]
$H'\,^3\Sigma_g^-$	38 328.248[c]	244.6(1.8)	1.80(29)			
$G^3\Pi_{og}$	34 519.697(4)[c]	237.5(1.9)	0.41(46)	0.160 25(18)[c,d]	0.001 10(14)[c]	2.7924(16)[d]
$F3\,^3\Sigma_g^-$	32 598.8 (7)	209.83(35)	1.15 (3)			[2.825][a]
F'	31 101.6(1.2)	243.3(1.1)	5.85(15)			
F''	30 530.4(1.9)	129.9(2.0)	0.1 (3)			
$E'\,3\,^3\Pi_g$	28 036.0	551.8	11.7			[2.629][a]
$E\,2\,^3\Sigma_g^-$	27 274.7	199.58(30)	1.01(1)			2.99[e]
$2\,^3\Pi_g$	~24 500[f] (predissociated)	~240				[2.440][a]
$B\,1\,^3\Sigma_u^-$	17 231.25 + x[g]	278.80	0.831	0.1907(5)	0.0013(5)	2.5598(34)
$1^3\Pi_g$	~15 000[h] (repulsive)					
$A\,1\,^3\Sigma_g^-$	x[g]	350.01	2.022	0.2054(4)	0.0012(4)	2.4665(24)
$^3\Pi_{2u}$	63.4					
$X\,^3\Pi_{1u}$	30.4			0.17127(19)[i]	0.0008(3)[i]	2.7011(15)[i]
$X\,^3\Pi_{0^+u}$	0.0433(10)	285.8	0.9			
$X\,^3\Pi_{0^-u}$	−0.0433(10)	285.8	0.9			

[a] All values except for r_e are reported in wave numbers (cm^{-1}). Error limits are quoted as one standard deviation and are given in parentheses following each entry in the table. The numbers in parentheses give the estimated error in the last reported digits of the reported value. Values in square brackets are based on the theoretical calculations of Ref. 31.

[b] T_0 gives the energy of the $v = 0$ level of the given electronic state relative to the energy of the $v = 0$ level of the ground $X\,^3\Pi_{ou}$ level.

[c] Measured in high resolution using the well known absorption lines of I_2 (Refs. 27 and 28) for calibration, and corrected for the Doppler shift experienced by the molecular beam as it moves toward the light source.

[d] For this state the value of B_e is uncorrected for spin uncoupling effects since the spin–orbit constant A is unknown. When this effect in included B_e will increase and r_e will decrease, perhaps by as much as 2%.

[e] Estimated by rotational contour analysis in Ref. 7.

[f] Observed in rare gas matrices in Refs. 3 and 4.

[g] Observed as the $B\ 1\,^3\Sigma_u^- \rightarrow A\ 1\,^3\Sigma_g^-$ emission system in gaseous Al_2 in Refs. 1 and 2.

[h] Observed in Al_2 isolated in solid krypton in Ref. 3.

[i] Corrected for spin uncoupling effects as described in Sec. IV; also corrected from B_0 to B_e (and r_0 to r_e) using α_e estimated from the Pekeris relationship. See Sec. IV A 1 for details.

ponent (Ω) of the $X\,^3\Pi_u$ state by the amount

$$E^{(2)}(^3\Pi_u,\Omega) = \frac{|\langle Y,\Omega|\hat{H}_{so}|^3\Pi_u,\Omega\rangle|^2}{E(^3\Pi_u,\Omega) - E(Y,\Omega)}, \qquad (4.1)$$

where $\hat{H}_{so}$ is the spin–orbit portion of the Hamiltonian. The observed asymmetry in the spin–orbit intervals may best be explained by the assumption that the $^3\Pi_u$ ($\Omega = 1$) state has been preferentially lowered in energy through such interactions. Of the various low-lying electronic states which have been calculated,[31] the $^1\Pi_u$ state arising from the same $\sigma_g^1\pi_u^1$ configuration as the ground $X\,^3\Pi_u$ state is most likely the cause of the spin–orbit asymmetry. This $^1\Pi_u$ state possesses $\Omega = 1$ only, and will therefore only affect the $\Omega = 1$ component of the $X\,^3\Pi_u$ state. Moreover, it is the only state of u symmetry calculated within 13 000 cm^{-1} of the ground $X\,^3\Pi_u$ state, and is therefore the only state within this range which may perturb the ground state. Using the methods described by Lefebvre-Brion and Field,[34] the numerator of Eq. (4.1) may be estimated as

$$|\langle\sigma_g^1\pi_u^1,{}^1\Pi_u,\Omega = 1|\hat{H}_{so}|\sigma_g^1\pi_u^1,{}^3\Pi_u,\Omega = 1\rangle| = 31.65\ cm^{-1},$$

where the value of the overlap integral S_{AB} has been taken to be 0.18, as found in Sec. III. Assuming that the entire spin–orbit asymmetry of the $X\,^3\Pi_u$ state arises from the $^3\Pi_u$, $\Omega = 1 \sim {}^1\Pi_u$, $\Omega = 1$ interaction then requires $E^{(2)}(^3\Pi_u,\Omega = 1) = -1.30\ cm^{-1}$. This in turn places the $\sigma_g^1\pi_u^1$, $^1\Pi_u$ state 770 cm^{-1} above the $X\,^3\Pi_u$ ($\Omega = 1$) state. Allowing for errors in the measured spin–orbit intervals and the possibility of significant couplings to higher-lying states, a more conservative estimate of the location of the $^1\Pi_u$ state places it in the range of $1000 \pm 300\ cm^{-1}$ above the ground state. This is in fair agreement with its calculated[31] energy of 3343 cm^{-1}, particularly in view of the difficulties involved in computing the energy of singlet and triplet states to the same degree of accuracy.

The Λ doubling of the $X\,^3\Pi_{ou}$ ground state, which splits the $\Omega = 0$ level into 0_u^+ and 0_u^- states, is also a consequence of off-diagonal spin–orbit interactions with higher-lying states. In this case, however, the splitting can only arise from interactions with Σ_u states, since states with $\Lambda \neq 0$ will perturb both 0_u^+ and 0_u^- components equally. The experimental observation that 0_u^- state lies below the 0_u^+ state then implies that off-diagonal couplings between the $X\,^3\Pi_{ou}$ state and states containing 0_u^- components ($^1\Sigma_u^-$ and $^3\Sigma_u^+$) are stronger than the couplings to states with 0_u^+ components ($^1\Sigma_u^+$ and $^3\Sigma_u^-$). Although it is not so straightforward to calculate matrix elements in these cases, the sense of the experimentally determined 0_u^+–0_u^- splitting is in agreement with theory, since theory places more 0_u^- perturbers at lower energies [$^1\Sigma_u^-$ at 11 000 cm^{-1} (repulsive); $^3\Sigma_u^+$ at 14 371

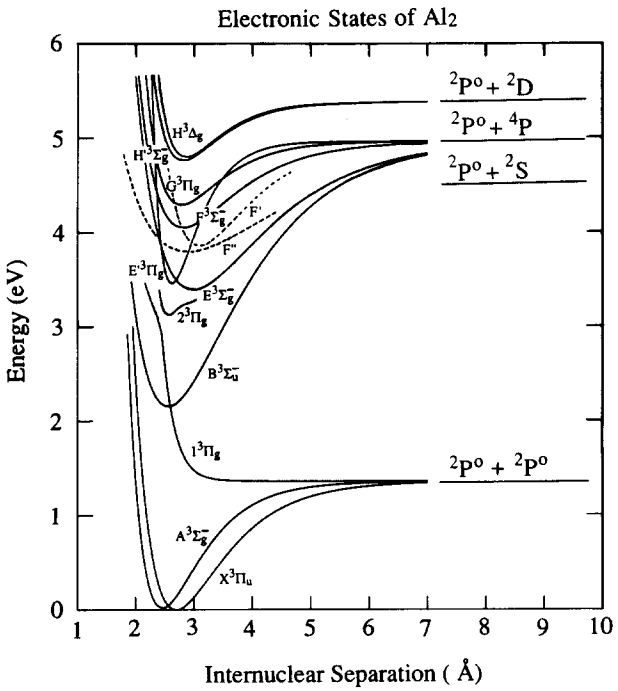

FIG. 11. Schematic potential energy curves for the experimentally known electronic states of Al_2. Potential curves, based on the Morse potential, are drawn using the parameters given in Table VII, with the anharmonicities altered to force dissociation to appropriate separated atom limits. The F' and F'' states are indicated as dashed curves because the $v = 0$ levels of these states have not been located with certainty, so none of the parameters T_0, ω_e, or r_e are accurately known. The shape of the $2\,^3\Pi_g$ curve is based on theoretical results from Ref. 31.

cm^{-1} (repulsive); $^1\Sigma_u^-$ at 29 000 cm^{-1}] than 0_u^+ perturbers ($B\,^3\Sigma_u^-$ at 17 120 cm^{-1}; $^3\Sigma_u^-$ at 25 102 cm^{-1}; $^1\Sigma_u^+$ at 27 838 cm^{-1}).[31]

The bond length of the ground state of Al_2 may be estimated from the value of $B_0(X\,^3\Pi_u, \Omega = 0)$. Before this can be done properly, however, the effects of spin uncoupling must be removed. According to Herzberg,[32] the effective rotational constant for a triplet state is given by

$$B_{\text{eff}} = B(1 + 2B\Sigma/A\Lambda), \tag{4.2}$$

where B is the true rotational constant and A is the spin–orbit interaction parameter. Using $A = 31.7$ cm^{-1} (as determined in Sec. III) and $B_{\text{eff}}(X\,^3\Pi_u, \Omega = 0, v = 0) = 0.169\,03$ cm^{-1}, one obtains $B_0 = 0.170\,87 \pm 0.000\,11$ cm^{-1}, from which a bond length of $r_0 = 2.7042 \pm 0.0008$ Å may be derived. Finally, Bondybey's values[7] of $\omega_e = 285.8$ cm^{-1}, and $\omega_e x_e = 0.9$ cm^{-1} may be used with the Pekeris relationship[32] to estimate B_e and α_e as $B_e = 0.171\,27 \pm 0.000\,19$ cm^{-1} and $\alpha_e = 0.0008 \pm 0.0003$ cm^{-1}. This then provides a final estimate of r_e ($X\,^3\Pi_u$) of 2.7011 ± 0.0015 Å. This value is similar to the *ab initio* bond lengths calculated by Sunil and Jordan[17] (2.717 Å), Bauschlicher *et al.*[16] (2.727 Å), and Upton[12] (2.72 Å).

2. The $A\,^3\Sigma_g^-$ state

The $A\,^3\Sigma_g^-$ state, arising from the π_u^2 molecular configuration, has remained unobserved in all jet-cooled spectroscopic investigations.[6,7] Our knowledge of this state derives entirely from the work of Ginter *et al.*[2] and from theoretical studies, where it is calculated to lie only 170 cm^{-1} above the $X\,^3\Pi_u$ state.[16,17] Spectroscopic constants are given in Table VII.

3. The $1\,^3\Pi_g$ state

The lowest state of $^3\Pi_g$ symmetry is calculated to be repulsive, having a region of Franck–Condon overlap with the ground state in the energy range near 15 000 cm^{-1}.[31] This corresponds nicely to a broad continuum absorption centered at 14 300 cm^{-1}, which was observed for Al_2 isolated in a solid krypton matrix by Douglas *et al.*[3] No other optically allowed transitions are expected in this region,[31] so this assignment appears definite.

4. The $B\,^3\Sigma_u^-$ state

The upper state of the Ginter band system[2] is calculated as the lowest state of $^3\Sigma_u^-$ symmetry.[31] As may be determined from Table VIII, this state must correlate to an excited separated atom limit (in this case, to the $s^2p, {}^2P^0 + sp^2, {}^4P$ limit, located 29 066.90 cm^{-1} above ground state atoms).

TABLE VIII. Separated atom limits and molecular states for Al_2.

Separated atom limit	Energy[a]	Molecular States[b]
$s^2p,{}^2P^0 + s^2p,{}^2P^0$	0	$X\,^3\Pi_u$, $A\,^3\Sigma_g^-$ $1\,^3\Pi_g$, $^3\Delta_u$, $^3\Sigma_u^+$ (2), $^1\Sigma_g^+$ (2), $^1\Sigma_u^-$, $^1\Pi_g$, $^1\Pi_u$, $^1\Delta_g$
$s^2p,{}^2P^0 + s^2s,{}^2S$	25 347.69	$2\,^3\Pi_g$, $^3\Pi_u$, $^3\Sigma_g^+$, $^3\Sigma_u^+$ $^1\Sigma_g^+$, $^1\Sigma_u^+$, $^1\Pi_g$, $^1\Pi_u$
$s^2p,{}^2P^0 + sp^2,{}^4P$	29 066.90	$^5\Sigma_g^+$, $^5\Sigma_u^+$, $^5\Sigma_g^-$ (2), $^5\Sigma_u^-$ (2), $^5\Pi_g$ (2), $^5\Pi_u$ (2), $^5\Delta_g$, $^5\Delta_u$, $E\,^3\Sigma_g^-$, $F\,^3\Sigma_g^-$, $E'\,^3\Pi_g$, $G\,^3\Pi_g$, $B\,^3\Sigma_u^-$, $^3\Sigma_u^-$, $^3\Sigma_g^+$, $^3\Sigma_u^+$, $^3\Pi_u$ (2), $^3\Delta_g$, $^3\Delta_u$
$s^2p,{}^2P^0 + s^2d,{}^2D$	32 435	$^3\Sigma_g^+$ (2), $^3\Sigma_u^+$ (2), $^3\Sigma_g^-$, $^3\Sigma_u^-$, $^3\Pi_g$ (3), $^3\Pi_u$ (3), $^3\Delta_g$ (2), $^3\Delta_u$ (2), $^3\Phi_g$, $^3\Phi_u$, $^1\Sigma_g^+$ (2), $^1\Sigma_u^+$ (2), $^1\Sigma_g^-$, $^1\Sigma_u^-$, $^1\Pi_g$ (3), $^1\Pi_u$ (3), $^1\Delta_g$ (2), $^1\Delta_u$ (2), $^1\Phi_g$, $^1\Phi_u$
$s^2p,{}^2P^0 + s^2p,{}^2P^0$	32 955	$^3\Sigma_g^+$ (2), $^3\Sigma_u^+$ (2), $^3\Sigma_g^-$, $^3\Sigma_u^-$, $^3\Pi_g$ (2), $^3\Pi_u$ (2), $^3\Delta_g$, $^3\Delta_u$, $^1\Sigma_g^+$ (2), $^1\Sigma_u^+$ (2), $^1\Sigma_g^-$, $^1\Sigma_u^-$, $^1\Pi_g$ (2), $^1\Pi_u$ (2), $^1\Delta_g$, $^1\Delta_u$

[a] Energies taken from Ref. 29.
[b] Molecular states derived using the Wigner–Witmer rules, as described in Ref. 32.

Therefore, the $B\,^3\Sigma_u^-$ state must be bound 11 835 cm^{-1} (29 066.90–17 231.25) more strongly than the $A\,^3\Sigma_g^-$ state. Presumably it is more strongly bound than the ground $X\,^3\Pi_u$ state by a comparable amount as well. This gives the $B\,^3\Sigma_u^-$ state a bond strength roughly double that of the ground state of Al_2, and clearly demonstrates the presence of multiple bonds in this state. Multiple bonding has become possible in this state because of the promotion of a 3*s* electron into the 3*p* shell on one atom, thereby allowing states with formal bond orders of 2 to be generated.

The $B\,^3\Sigma_u^-$ state must place two electrons in π orbitals, since this is the only way a Σ^- state can be obtained. The high bond strength of this state then implies a π_u^2 configuration for the π electrons, giving the molecule a full π bond in this state. Of the remaining four valence electrons, which are distributed in σ orbitals, only one may be in an orbital of *u* symmetry (otherwise a Σ_g^-, rather than a Σ_u^-, state is obtained). Thus, three σ electrons occupy bonding orbitals and one occupies an antibonding orbital, giving a σ bond order of one as well. With one full π bond and one full σ bond the high bond strength of this state, relative to its separated atom limit, is hardly surprising.

5. The $2\,^3\Pi_g$ state

Both Douglas *et al.*[3] and Abe and Kolb[4] report absorption spectra with vibrational structure in the range of 24 400–25 600 cm^{-1} for Al_2 isolated in Ar, Kr, or Xe matrices. Neither Cai *et al.*[7] nor we have been able to observe any transitions in this spectral range for jet-cooled gaseous Al_2, however. Langhoff and Bauschlicher[31] calculate the $2\,^3\Pi_g$ state of Al_2 to lie 23 054 cm^{-1} above the ground state, and have assigned the structured absorption spectra of Douglas *et al.*[3] and Abe and Kolb[4] to the $2\,^3\Pi_g \leftarrow X\,^3\Pi_u$ band system. The calculated [31] potential energy curve for the $2\,^3\Pi_g$ state displays an unusual, skewed shape, however, caused by avoided crossings between the $E'\,3\,^3\Pi_g$ (see below), $2\,^3\Pi_g$, and $1\,^3\Pi_g$ states. The potential energy curves of these states are of course calculated in the adiabatic approximation, and nonadiabatic couplings certainly exist between them. The failure to observe the $2\,^3\Pi_g \leftarrow X\,^3\Pi_u$ transition in gaseous Al_2 using laser-induced fluorescence[7] or resonant two-photon ionization methods may be plausibly accounted for if predissociation occurs on a more rapid time scale than either fluorescence or absorption of a second, ionizing photon. Nonadiabatic couplings between the $2\,^3\Pi g$ state and the repulsive $1\,^3\Pi_g$ state provide a straightforward mechanism for this predissociation. Based on the lack of an observable gas-phase LIF or R2PI signal for this band system, the predissociation rate must exceed $10^9\ s^{-1}$.

6. The $E\,2\,^3\Sigma_g^-$ state

The $E\,2\,^3\Sigma_g^- \leftarrow X\,^3\Pi_u$ band system of Al_2 was first reported in 1989 by Cai, Dzugan, and Bondybey.[7] If the $E'' \leftarrow X$ system displayed in Fig. 2 is accepted as comprising the higher vibrational transitions of the $E \leftarrow X$ system, our observations of this system then extend to much higher vibrational levels than were previously reported.[7] As discussed in Sec. III A, however, this assignment presents a few difficulties. In particular, the 10–0 band is extremely weak or missing, and the 13–0 band is anomalously weak as well.

A suggestion as to why certain bands may be anomalously weak is provided by the theoretical work of Langhoff and Bauschlicher,[31] which permitted the first definitive assignment of the upper state of this system as $^3\Sigma_g^-$. Close inspection of the calculated potential energy curves shows that the $E\,2\,^3\Sigma_g^-$ and $F\,3\,^3\Sigma_g^-$ (see below) electronic states undergo an avoided crossing near an internuclear separation of 2.9 Å, which corresponds to an energy of approximately 29 000 cm^{-1} for the $E\,2\,^3\Sigma_g^-$ state. The electronic transition moment calculated [31] for the $E\,2\,^3\Sigma_g^- \leftarrow X\,^3\Pi_u$ transition changes sign near this internuclear separation, presumably due to a destructive interference between the transition moments associated with the two diabatic states, which are mixed to generate the noncrossing, adiabatic states. Although one would require accurate potential energy curves and vibrational wave functions to prove the point, it is plausible that certain vibrational bands in the vicinity of this avoided crossing could display a vanishingly small intensity due to an accidental destructive interference between regions of space with positive electronic transition moments and ones with negative moments. Anomalous intensity patterns would then be expected to continue for higher energy bands of the $E\,2\,^3\Sigma_g^- \leftarrow X\,^3\Pi_u$ band system, because regions of both positive and negative electronic transition moments could still be accessed. The appearance of anomalous intensity patterns in the $E\,2\,^3\Sigma_g^- - X\,^3\Pi_u$ band system for v'–0 bands lying at or above 29 000 cm^{-1} is then consistent with the avoided crossing implied by *ab initio* calculations.

Cai *et al.*[7] have simulated rotational contours for the $E\,2\,^3\Sigma_g^- \leftarrow X\,^3\Pi_u$ band system, and have estimated $r_e(E\,2\,^3\Sigma_g^-) = 2.99$ Å and $r_e(X\,^3\Pi_u) = 2.70$ Å. The close correspondence between this estimate for $r_e(X\,^3\Pi_u)$ and the value obtained from rotationally resolved spectra in the present work lends support to the estimated value of $r_e(E\,2\,^3\Sigma_g^-)$ of 2.99 Å. This also compares favorably with the *ab initio*[31] estimate of 3.226 Å. A large change in bond length upon electronic excitation in the $E\,2\,^3\Sigma_g^- \leftarrow X\,^3\Pi_u$ system is also consistent with a long vibrational progression, as is observed in the present work.

7. The $E'\,3\,^3\Pi_g$ state

Within the spectral range of the $E\,2\,^3\Sigma_g^- \leftarrow X\,^3\Pi_u$ band system we find two intense bands and a third, weak band which belong to another band system. These are designated as the E'–X band system, which is much more intense than the $E\,2\,^3\Sigma_g^- \leftarrow X\,^3\Pi_u$ system. The spectrum shown in Fig. 1 provides a misleading impression of the relative intensities of the E–X and E'–X systems, since it was collected at high laser fluences, leading to significant saturation effects.

The E' state is noteworthy in several respects. First is the extreme intensity of the 0–0 band of the E'–X system, which is without a doubt the most intense band we have observed for Al_2 in any spectral region. What makes this intensity so remarkable is the near-total absence of both the 0–0 band (near 28 036 cm^{-1}) and the 1–0 band (near 28 564 cm^{-1}) in the laser-induced fluorescence spectra of Cai *et al.*[7] This

implies that the E'–X system is a strongly allowed transition, but that the fluorescence quantum yield is miniscule. Accordingly we may deduce that the E' predissociates on a time scale rapid compared to that of fluorescence, but short compared to the time required for absorption of a second, ionizing photon in the resonant two-photon ionization experiments.

A second unusual aspect of the E' state is its extremely large vibrational spacing ($\Delta G_{1/2} = 528.5$ cm^{-1}), which combined with the fact that the E'–X 0–0 band is shaded to the blue indicates a short bond length and a narrow potential well. Langhoff and Bauschlicher[31] calculate the $3\,^3\Pi_g$ state of Al_2 to lie 27 749 cm^{-1} above the $X\,^3\Pi_u$ state. This is quite close to the observed 0–0 band of the E'–X system, which lies near 28 036 cm^{-1}. Moreover, the *ab initio*[31] estimates of ω_e and r_e for the $3\,^3\Pi_g$ state (495 cm^{-1} and 2.629 Å) are in general agreement with the large value of $\Delta G_{1/2}$ which is experimentally observed and the short bond length which is inferred from the blue shading of the bands. Finally, the *ab initio* work[31] predicts that the $3\,^3\Pi_g \leftarrow X\,^3\Pi_u$ band system should be among the most intense of the band systems lying below 30 000 cm^{-1}. With this level of agreement between theory and experiment there can be little doubt that the E' state is the $3\,^3\Pi_g$ state predicted by theory.

As mentioned above, it is clear that the $E'\,3\,^3\Pi_g$ state of Al_2 undergoes rapid predissociation. Judging from the fact that this state is observable by resonant two-photon ionization, however, its predissociation cannot be as rapid as that of the $2\,^3\Pi_g$ state (discussed above), which is predissociated by nonadiabatic coupling to the repulsive $1\,^3\Pi_g$ state. As is evident from the *ab initio* potential energy curves reported by Langhoff and Bauschlicher,[31] avoided crossings are present between all three $^3\Pi_g$ curves. Presumably the same nonadiabatic couplings that cause the $2\,^3\Pi_g$ state to predissociate extremely rapidly also cause the $E'\,3\,^3\Pi_g$ state to predissociate as well, with Al_2 ultimately falling apart through the repulsive $1\,^3\Pi_g$ state.

8. The F″ state

As shown in Fig. 3, the F''–X band system is found between the high v'–0 bands of the E–X system and the F'–X system. The system is quite irregular, and several extra, unexplained bands are present in this energy region. At this point no definite assignment of the F'' state is possible.

9. The F′ state

As shown in Fig. 4, the F'–X band system consists of regular triplets of subbands with a spacing similar to that found in the E–X and F–X (see below) band systems. This would imply a small spin–orbit splitting in the upper state, suggesting that the F' state probably belongs to Hund's case (b). The intensity of the individual bands grows as one moves to higher frequencies, in a manner which suggests a large increase in internuclear separation upon electronic excitation. The more intense bands also show an obvious degradation to the red, clearly establishing that $r_e(F') > r_e(X\,^3\Pi_u)$. The intensity of the band system is quite low compared to other band systems, and above 32 500 cm^{-1} this system is obscured by the much more intense $F\,^3\Sigma_g^- \leftarrow X\,^3\Pi_u$ system. No definite assignment of this system is possible at the present time.

10. The F 3 $^3\Sigma_g^-$ state

The $F\,3\,^3\Sigma_g^- \leftarrow X\,^3\Pi_u$ band system of Al_2 was first reported in 1989 by Cai, Dzugan, and Bondybey.[7] The bands observed are again red-degraded, but the vibrational progression is not nearly as extensive as that found for the $E\,2\,^3\Sigma_g^- \leftarrow X\,^3\Pi_u$ system. This implies that the bond length of the $F\,3\,^3\Sigma_g^-$ state lies between that of the $X\,^3\Pi_u$ state (2.701 Å) and that of the $E\,2\,^3\Sigma_g^-$ state (2.99 Å). High resolution spectroscopic data is not yet available to confirm this expectation.

Assignment of the symmetry of the F state as $^3\Sigma_g$ is reasonable based on a confirmed ground state assignment of $^3\Pi_u$ and the measured spin–orbit intervals. The assignment of the + or − character of this $^3\Sigma_g$ state, however, is based entirely on theoretical work by Langhoff and Bauschlicher,[31] who calculate the $3\,^3\Sigma_g^-$ state of Al_2 to lie 32 041 cm^{-1} above the ground $X\,^3\Pi_u$ state. This value is in excellent agreement with the frequency of the 0–0 band of the F–X system, allowing the F state to be identified with the computed $3\,^3\Sigma_g^-$ state.

11. The G $^3\Pi_g$ state

Near 34 520 cm^{-1} one find the G–X 0–0 band, which has been shown in Sec. III to correspond to a $^3\Pi_g \leftarrow X\,^3\Pi_u$ electronic transition. It is a measure of the electronic complexity of Al_2 that this is the fourth known electronic state of $^3\Pi_g$ symmetry within 35 000 cm^{-1} of the ground molecular state. Other than the state symmetry, bond length, and vibrational frequency, little is known about the $G\,^3\Pi_g$ state. It lies above the region reliably computed by Langhoff and Bauschlicher,[31] and may quite possibly have significant contributions from the $3s^2 3p^1\,{}^2P^0 + 3s^2 3d^1\,{}^2D$ separated atom limit, which lies 32 435 cm^{-1} above ground state atoms. As is obvious from Table VIII, a large number of electronic states arise from this separated atom limit, and it has not yet been possible to include the Al $3d$ shell in the active space of a CASSCF calculation.[31] As a result, no reliable theoretical work on the $G\,^3\Pi_g$ or higher lying states of Al_2 yet exists.

12. The H′ $^3\Sigma_g^-$ state

As described in the previous section, the H' state has been conclusively shown to be of $^3\Sigma_g^-$ symmetry. Its rotational energy levels are not well described by the standard model, however, indicating that it is seriously perturbed by other states. As a result it cannot be described using a single rotational constant, presumably because of strong off-diagonal perturbations induced by the L-uncoupling and S-uncoupling operators. As a result it is impossible to use the measured rotational constants to estimate the bond length in this state.

13. The H $^3\Delta_g$ state

The highest energy electronic state yet characterized for Al_2 is the $H\,^3\Delta_g$ state, which was investigated in high resolution as described in Sec. III. Apart from the term symbol,

bond length, and vibrational frequency, little is known concerning this state. By allowing the ground $X\,^3\Pi_u$ state $\Omega = 0_u^+, 0_u^-$ splitting to be measured, however, the $H\,^3\Delta_g \leftarrow X\,^3\Pi_u$ transition has contributed significantly to our understanding of Al_2, and has provided the most definite evidence that the ground state is of $^3\Pi_u$ symmetry. Spectroscopic constants for the $H\,^3\Delta_g$ state are given in Table VII.

B. The bond strength of Al_2

A number of investigators have estimated the bond strength of Al_2 by Knudsen effusion mass spectrometry.[40–43] The most careful study appears to have been performed by Stearns and Kohl in 1972.[43] These authors have based their investigation on the gaseous equilibria

$$\mathrm{AlAu(g) + Al(g) \overset{K_1}{\rightleftarrows} Al_2(g) + Au(g)} \tag{4.3}$$

and

$$\mathrm{2AlAu(g) \overset{K_2}{\rightleftarrows} Al_2(g) + Au_2(g)}, \tag{4.4}$$

which have been measured at temperatures in the range of 1921–2032 K. Unlike previous investigators, these authors have meticulously subtracted background signals at mass 54 ($^{54}Fe^+$, $^{54}Cr^+$, and $^{27}Al_2^+$ fragments produced from Al_2O) to correct the measured concentration of Al_2. Failure to make this correction leads to a systematic overestimate of the Al_2 concentration in the Knudsen cell, leading to an overestimate of the Al_2 bond strength. Stearns and Kohl[43] then used the measured equilibrium constants K_1 and K_2 to evaluate the enthalpy change in reactions (4.3) and (4.4) by both the second-law and third-law methods. The second-law method uses the temperature variation of the measured equilibria to extract ΔH for each reaction, and is subject to significant errors when only a small temperature range is investigated. The third-law method uses statistical thermodynamic expressions for the equilibria to obtain ΔH_0^0 for each reaction, and has the potential of greater accuracy. Improved accuracy is only achievable in the third-law method if the molecular partition functions may be reliably estimated at the high temperatures of the experiment, however. This becomes particularly difficult for molecules with large numbers of low-lying, poorly characterized states. As one might expect, Al_2 certainly fell into this category when the experiments were performed in 1972.[43]

We have used the values of K_1 and K_2 reported by Stearns and Kohl[43] to reevaluate the third-law value of $D_0^0(Al_2)$ in light of the new information available about Al_2. To limit the possibility of errors, the somewhat poorly known molecule AlAu has been eliminated by considering the equilibrium

$$\mathrm{2Al(g) \overset{K_{Al}}{\rightleftarrows} Al_2(g)}. \tag{4.5}$$

It may be readily shown that

$$K_{Al} = (K_1^2/K_2)[P(Au_2)/P(Au)^2] \tag{4.6}$$

or

$$K_{Al} = (K_1^2/K_2)K_{Au}, \tag{4.7}$$

where K_{Au} refers to the dimerization of gold:

$$\mathrm{2Au(g) \overset{K_{Au}}{\rightleftarrows} Au_2(g)}. \tag{4.8}$$

The bond energy[44–46] and spectroscopic constants[47–49] of Au_2 are accurately known, so K_{Au} may be accurately calculated from statistical thermodynamics.[50] With the aid of Eq. (4.7) and the measured values of K_1 and K_2, the equilibrium constant for the dimerization of aluminum may be readily computed. Finally, the statistical thermodynamic expression for K_{Al} may be used to obtain $D_0^0(Al_2)$ as

$$\begin{aligned} D_0^0(Al_2) = {} & D_0^0(Au_2) + \frac{3}{2}kT\ln\frac{m_{Al}}{m_{Au}} + 2kT\ln\left(\frac{q(Al)}{q(Au)}\right) \\ & + kT\ln(K_1^2/K_2) + kT\ln\left[\sum_i \frac{g_i(Au_2)\,\exp[-\Delta E_i(Au_2)]}{B_i(Au_2)\{1-\exp[-\hbar\omega_i(Au_2)/kT]\}}\right] \\ & - kT\ln\left[\sum_i \frac{g_i(Al_2)\,\exp[-\Delta E_i(Al_2)]}{B_i(Al_2)\{1-\exp[-\hbar\omega_i(Al_2)/kT]\}}\right]. \end{aligned} \tag{4.9}$$

In this expression m_{Al} and m_{Au} are the atomic masses of aluminum and gold, respectively, $q(Al)$ and $q(Au)$ are the electronic partition functions of atomic aluminum and gold, respectively (which are easily evaluated from atomic data[29]), and K_1 and K_2 are the equilibrium constants reported by Stearns and Kohl[43] for reactions (4.3) and (4.4), respectively. The summations run over all thermally accessible electronic states of Au_2 and Al_2, respectively, with g_i giving the electronic degeneracy of the state, B_i giving its rotational constant, ΔE_i giving its electronic energy relative to the ground electronic state, and ω_i giving its vibrational frequency. In this expression only one term contributes significantly to the sum over states for Au_2, since the first excited state of Au_2 lies approximately 16 000 cm^{-1} above the ground state.[46]

We have evaluated the sum over states for Al_2 in Eq. (4.9) using the energies and spectroscopic constants of the low-lying states of Al_2 as reported by Langhoff and Bauschlicher.[31] To estimate the sensitivity of the result on the calculated electronic energies we have also evaluated the expression (1) with all of the singlet states reported by Langhoff and Bauschlicher shifted 2000 cm^{-1} lower in energy, and (2) with all of the singlets shifted 1000 cm^{-1} higher in energy and with the $A\,^3\Sigma_g^-$ state shifted 500 cm^{-1} higher in

energy. The final result gives $D_0^0(Al_2) = 1.34 \pm 0.06$ eV, with the error limits encompassing the standard deviation of the measured data points (from Ref. 43) as well as the uncertainty associated with the energies of the low-lying electronic states of Al_2, as estimated above.

The revised value of $D_0^0(Al_2) = 1.34 \pm 0.06$ eV is considerably lower than previous estimates [1.96 ± 0.43 eV (Ref. 40, as recalculated in Ref. 42); 1.67 – 1.80 eV (Ref. 41); 1.78 ± 0.19 eV (Ref. 42); and 1.55 ± 0.15 eV (Ref. 43)]. As mentioned above, some of these studies overestimated the bond strength of Al_2 because they failed to subtract the background signal due to other species of mass 54. In addition, all of the previous studies seriously underestimated the partition function of $Al_2(g)$, since they only considered the $A\,^3\Sigma_g^-$ state to be thermally populated at 2000 K.

The revised bond strength of Al_2, 1.34 ± 0.06 eV, is in agreement with the bond strengths obtained in the most extensively correlated calculations, which give $D_0^0(Al_2) = 1.369$ eV[16] and 1.33 eV.[17] It is also very close to the value reported by Upton in a GVB study with extensive configuration interaction (1.31 eV).[12] It appears that *ab initio* theory is currently capable of describing the electronic structure of molecules as complicated as Al_2 with high accuracy, provided large basis sets and extensive configuration interaction are included.

The recently measured value of the adiabatic ionization potential of Al_2 [$IP(Al_2) = 5.989 \pm 0.002$ eV][26] may be combined with the value of $D_0^0(Al_2)$ given above and the atomic ionization potential of Al (5.984 eV)[29] to obtain the bond strength of Al_2^+ as $D_0^0(Al_2) = 1.34 \pm 0.06$ eV. This is somewhat greater than the value obtained by Hanley, Ruatta, and Anderson[51] in a collision-induced dissociation experiment (0.90 ± 0.30 eV). It is in good agreement with the bond strengths calculated by *ab initio* theory, however, with Sunil and Jordan[17] reporting $D_0^0(Al_2^+) = 1.36$ eV, and Bauschlicher *et al.*[52] reporting $D_0^0(Al_2^+) = 1.41$ eV.

V. CONCLUSION

The ground state of Al_2 has been conclusively demonstrated to be of $^3\Pi_u$ symmetry, deriving from the $\sigma_g^1\pi_u^1$ electronic configuration. Rotationally resolved investigations have allowed the bond length of the $X\,^3\Pi_u$ state of Al_2 to be measured as $r_e(X\,^3\Pi_u) = 2.701 \pm 0.002$ Å. The lambda doubling which splits the $X\,^3\Pi_u$, $\Omega = 0_u^+, 0_u^-$ pair of substates has been resolved, and the 0_u^- substate is found to lie 0.08 cm^{-1} lower in energy than the 0_u^+ substate. An asymmetry in the measured spin–orbit intervals of the $X\,^3\Pi_u$ state suggests that the observed $\sigma_g^1\pi_u^1$, $^1\Pi_u$ state lies about 1000 cm^{-1} above the ground state. The measured spectroscopic constants of the ground $X\,^3\Pi_u$ state have been used in combination with the calculated[31] properties of the low-lying electronic states to reevaluate the third-law estimate[43] of the Al_2 bond strength, providing a revised value of $D_0^0(Al_2) = 1.34 \pm 0.06$ eV. With Weisshaar's recent measurement[26] of the adiabatic ionization potential of Al_2, this also provides $D_0^0(Al_2) = 1.34 \pm 0.06$ eV. These values are substantially in agreement with the most extensively correlated calculations on Al_2.[16,17,52]

In addition to the $E\ 2\,^3\Sigma_g^- \leftarrow X\,^3\Pi_u$ and $F\,3\,^3\Sigma_g^- \leftarrow X\,^3\Pi_u$ band systems previously reported,[7] the $E'\ 3\,^3\Pi_g \leftarrow X\,^3\Pi_u$, $F'' \leftarrow X$, $F' \leftarrow X$, $G\,^3\Pi_g \leftarrow X\,^3\Pi_u$, $H'\,^3\Sigma_g^- \leftarrow X\,^3\Pi_u$, and $H\,^3\Delta_g \leftarrow X\,^3\Pi_u$ band systems have been observed for the first time. Rotational constants and electronic state symmetries have been determined for the $G\,^3\Pi_g$, $H'\,^3\Sigma_g^-$, and $H\,^3\Delta_g$ states by high resolution optical spectroscopy. A discussion of all of the experimentally known states of Al_2 has been presented, along with comparisons to previous experimental and theoretical work. Our understanding of the excited states of Al_2 has been aided immensely by the interplay between experiment and *ab initio* theory, particularly by the theoretical investigation of the excited states of Al_2 recently published by Langhoff and Bauschlicher.[31] This study has been used to identify the $E'\ 3\,^3\Pi_g$ state in the absence of rotationally resolved spectra, and also cleanly explains why certain states (the $2\,^3\Pi_g$ and $E'\,3\,^3\Pi_g$ states in particular) predissociate on a rapid time scale.

ACKNOWLEDGMENTS

We wish to thank Dr. C. W. Bauschlicher, Jr. and Professor Vladimir E. Bondybey for communicating their results to us prior to publication. We are grateful to Professor William H. Breckenridge for the use of the intracavity etalon and accessories employed in the high resolution investigations. We also gratefully acknowledge research support from the National Science Foundation under Grant No. CHE-8912673. Acknowledgment is also made to the donor of the Petroleum Research Fund, administered by the American Chemical Society, for partial support of this research.

[1] P. B. Zeeman, Can. J. Phys. **32**, 9 (1954).
[2] D. S. Ginter, M. L.Ginter, and K. K. Innes, Astrophys. J. **139**, 365 (1963).
[3] M. A. Douglas, R. H. Hauge, and J. L. Margrave, J. Phys. Chem. **87**, 2945 (1983).
[4] H. Abe and D. M. Kolb, Ber. Bunsenges. Phys. Chem. **87**, 523(1983).
[5] D. M. Cox, D. J. Trevor, R. L. Whetten, E. A. Rohlfing, and A. Kaldor, J. Chem. Phys. **84**, 4651 (1986).
[6] Z.-W. Fu, G. W. Lemire, Y. Hamrick, S. Taylor, J.-C. Shui, and M. D. Morse, J. Chem. Phys. **88**, 3524 (1988).
[7] M. F. Cai, T. P. Dzugan, and V. E. Bondybey, Chem. Phys. Lett. **155**, 430 (1989).
[8] N. H. Sabelli, R. Benedek, and T. L. Gilbert, Phys. Rev. A **20**, 677 (1979).
[9] M. Leleyter and P. Joyes, J. Phys. B **13**, 2165 (1980).
[10] D. J. Fox and H. F. Schaefer III, J. Chem. Phys. **78**, 328 (1983).
[11] J. S. Tse, J. Mol. Struct. (Theochem.) **165**, 21 (1988).
[12] T. H. Upton, J. Phys. Chem. **90**, 754 (1986).
[13] S. Lamson and R. Messmer, Chem. Phys. Lett. **98**, 72 (1983).
[14] G. Pacchioni, Theoret. Chim. Acta (Berlin) **62**, 461 (1983).
[15] H. Basch, W. J. Stevens, and M. Krauss, Chem. Phys. Lett. **109**, 212 (1984).
[16] C. W. Bauschlicher, Jr., H. Partridge, S. R. Langhoff, P. R. Taylor, and S. P. Walch, J. Chem. Phys. **86**, 7007 (1987).
[17] K. K. Sunil and K. D. Jordan, J. Phys. Chem. **92**, 2774 (1988).
[18] C. M. Quinn and M. E. Schwartz, J. Chem. Phys. **74**, 5151 (1981).
[19] A. D. McLean, B. Liu, and G. S. Chandler, J. Chem. Phys. **80**, 5130 (1984).
[20] S. Taylor, G. W. Lemire, Y. Hamrick, Z.-W. Fu, and M. D. Morse, J. Chem. Phys. **89**, 5517 (1988).
[21] G. W. Lemire, Z.-W. Fu, Y. Hamrick, S. Taylor, and M. D. Morse, J. Phys. Chem. **93**, 2313 (1989).
[22] Z.-W. Fu and M. D. Morse, J. Chem. Phys. **90**, 3417 (1988).
[23] G. W. Lemire, G. A. Bishea, S. A. Heidecke, and M. D. Morse, J. Chem. Phys. **92**, 121 (1990).

[24]S. Taylor, E. M. Spain, and M. D. Morse, J. Chem. Phys. **92**, 2698 (1990).
[25]S. C. O'Brien, Y. Liu, Q. Zhang, J. R. Heath, F. K. Tittel, R. F. Curl, and R. E. Smalley, J. Chem. Phys. **84**, 4074 (1986).
[26]J. E. Harrington and J. C. Weisshaar, J. Chem. Phys. **93**, 854 (1990).
[27]S. Gerstenkorn and P. Luc, *Atlas du Spectre d'Absorption de la Molécule d'Iode* (CNRS, Paris, 1978).
[28]S. Gerstenkorn and P. Luc, Rev. Phys. Appl. **14**, 791 (1979).
[29]C. E. Moore, Natl. Bur. Stand. Circ. 467 (US GPO, Washington, D.C., 1949, 1952).
[30]C. W. Bauschlicher, Jr. and S. R. Langhoff, J. Chem. Phys. **90**, 4627 (1989).
[31]S. R. Langhoff and C. W. Bauschlicher, Jr., J. Chem. Phys. **92**, 1879 (1990).
[32]G. Herzberg, *Molecular Spectra and Molecular Structure I. Spectra of Diatomic Molecules*, 2nd ed. (Van Nostrand Reinhold, New York, 1950).
[33]E. Ishiguro and M. Kobori, J. Phys. Soc. Jpn. **22**, 263 (1967).
[34]H. Lefebvre-Brion and R. W. Field, *Perturbations in the Spectra of Diatomic Molecules* (Academic, Orlando, FL, 1986).
[35]M. Tinkham, *Group Theory and Quantum Mechanics* (McGraw-Hill, New York, 1964), pp. 252–255.
[36]K. Balasubramanian and J. Li, J. Chem. Phys. **88**, 4979 (1988).
[37]J. M. Brown and A. J. Merer, J. Mol. Spectrosc. **74**, 488 (1979).
[38]J. M. Brown, A. S.-C. Cheung, and A. J. Merer, J. Mol. Spectrosc. **124**, 464 (1987).
[39]J. T. Hougen, *The Calculation of Rotational Energy Levels and Rotational Line Intensities in Diatomic Molecules*, Nat. Bur. Stand Monograph 115 (US GPO, Washington, D.C., 1970).
[40]W. A. Chupka, J. Berkowitz, C. F. Giese, and M. G. Inghram, J. Phys. Chem. **62**, 611 (1958).
[41]G. D. Blue and K. A. Gingerich, presented at the Sixteenth Annual Conference on Mass Spectrometry and Allied Topics, ASTM E-14, paper No. 129, Pittsburgh, PA, 1968.
[42]O. M. Uy and J. Drowart, Trans. Faraday Soc. **67**, 1293(1971).
[43]C. A. Stearns and F. J. Kohl, High Temp. Sci. **5**, 113 (1973).
[44]M. D. Morse, Chem. Rev. **86**, 1049–1109 (1986).
[45]J. Kordis, K. A. Gingerich, and R. J. Seyse, J. Chem. Phys. **61**, 5114 (1974).
[46]G. A. Bishea and M. D. Morse, Chem. Phys. Lett. **171**, 430 (1990).
[47]J. Ruamps, Ann. Phys. (Paris) **4**, 1111 (1959).
[48]B. Kleman, S. Lindqvist, and L. E. Selin, Ark. Fys. **8**, 505 (1954).
[49]L. L. Ames and R. F. Barrow, Trans. Faraday Soc. **63**, 39 (1967).
[50]D. A. McQuarrie, *Statistical Thermodynamics* (Harper&Row, New York, 1973).
[51]L. Hanley, S. A. Ruatta, and S. L. Anderson, J. Chem. Phys. **87**, 260 (1987).
[52]C. W. Bauschlicher, Jr., L. A. Barnes, and P. R. Taylor, J. Phys. Chem. **93**, 2932 (1989).